Contrast Formation in the SEM

3

An electron beam is rastered across the specimen surface resulting in the generation of secondary and backscattered electrons which are used to form images while x-rays are used to obtain elemental constitution of the specimen material. Present-day technology allows imaging of features as small as 1 nm in the SEM. The predominant use of the SEM is to generate SE and BSE images showing topographic and compositional contrast, respectively. This chapter deals with the mechanism of contrast formation, factors that affect its development, and how its interplay contributes to the appearance of various features observed in the images.

3.1 Image Formation

The electron gun located at the topmost section of the column generates an electron beam with an energy range of few hundred eV to 30 keV, which is focused into a fine probe by electromagnetic lenses located within the column. The fine electron probe is then rastered over specimen surface in a rectangular area by scan coils also present within the column. The scanned sample sits in the chamber located at the end of the microscope column. The gun, the column, and the specimen chamber are kept under vacuum to allow the electron beam to travel through the column and interact with the specimen. The electron beam penetrates into the specimen in the form of a teardrop extending from 100 nm to 5 μm depending on beam energy and specimen density. Interaction of beam with the specimen produces a variety of signals including secondary and backscattered electrons and x-rays, which are collected and used to produce images as well as to determine the elemental composition of the specimen material. In present-day microscopes, images are digitally processed, displayed on computer screens, and saved on hard drives.

© Springer Nature Switzerland AG 2018, Corrected Publication 2023

A. Ul-Hamid, *A Beginners' Guide to Scanning Electron Microscopy*,
https://doi.org/10.1007/978-3-319-98482-7_3

3.1.1 Digital Imaging

The electron probe with a specific diameter, current, and convergence angle is scanned from one point to the other across the specimen surface. In a digital scan, the probe dwells at a discrete location on the specimen for a set duration before it moves on. The electrons emanating from a discrete location are detected by the detector as a signal with a specific intensity. Each of these discrete locations, therefore, has stored values of x and y (position) and I (intensity). For each point where the electron beam interacts with the specimen and produces a signal, a corresponding point on the viewing screen (at x, y) is exhibited with intensity I. The detector acts as an interface between the signal emitted from the specimen and the corresponding image displayed on the screen. The level of brightness of the point on the display monitor is proportional to the strength of the signal emanating from the corresponding point in the specimen as measured and amplified by the detector. High signal strength from a location in the specimen will result in greater intensity at the corresponding location on the screen. The image on the screen, therefore, represents an intensity distribution map of the electron signals derived from the specimen. During imaging, the signal strength is proportional to the number of electrons ejected from a point on the specimen. During EDS analysis, the magnitude of the signal corresponds to the number of characteristic x-rays emitted from that discrete location and is indicative of the concentration of chemical element at that location. The length (L_{monitor}) of the scan on the viewing monitor is larger than the actual scan length (L_{specimen}) on the specimen resulting in magnification of the image that equals $\frac{L_{\text{monitor}}}{L_{\text{specimen}}}$ (Eq. 2.22). As shown in Fig. 3.1a one-to-one correspondence is established between the beam impact points on the specimen surface and the points on the display screen.

Discrete beam locations on the specimen from where the signal is generated are called *picture elements* with a roughly corresponding number of *pixels* in the image displayed on the viewing screen. The analog signal obtained from each picture element of the specimen is measured, amplified, and converted into a voltage signal by the detector electronics. It is then fed into an image processor board with an integrated analog-to-digital converter (ADC) and video control unit. The voltage signal is digitized into a video signal for each picture element, which is assigned a digital address with a specific numeric value (called the *index*) related to its x, y, I value. The video signal is then fed into the video capture card installed in the computer. The digital video signal is processed by this card to be displayed through a graphical user interface (GUI) on the flat panel screen typically used at present. Later it can be saved in various image formats in a variety of recording media. During the digitization process, each pixel is assigned a value for detected signal electronically which determines its intensity level. This is accomplished by assigning a gray level to each pixel. Typically, 256 gray levels are possible when working with 8 bit (i.e., $2^8 = 256$) information systems. The gray level of 0 is assigned for black and 256 for white, and the rest of the numbers represent various levels of gray. The human eye can discern up to 20 shades of gray only. Thus, 256 gray levels are deemed more

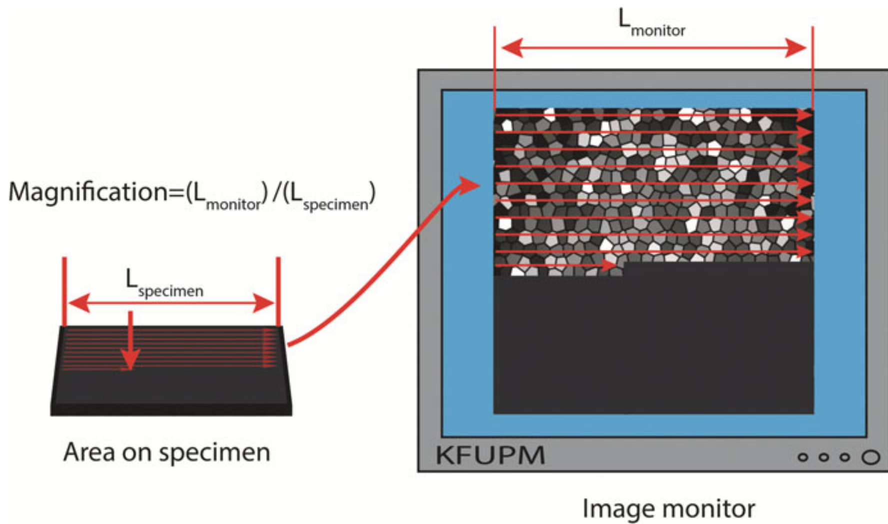

Fig. 3.1 Schematic illustrating the one-to-one correspondence between the beam locations on the specimen and the points on the monitor. Magnification is the scan length of the monitor to that of the specimen, i.e., $\frac{L_{monitor}}{L_{specimen}}$

than adequate for producing good-quality images. The number of pixels used in the image is specified as the digital image resolution such as 512 × 512, 1024 × 1024, etc. The image with 512 × 512 pixels will have 512 pixels in the horizontal direction and 512 pixels in the vertical direction. A higher number of pixels per unit area will produce images with higher resolution with correspondingly large file size.

A range of scan rates is available to the user to allow from slow to medium to fast scans. Initially, the specimen can be scanned quickly (several image frames per second) to search for the area of interest. Once the feature of interest has been located, the scan rate can be slowed down to several seconds per frame to capture a noise-free image. The dwell time at each location should be sufficient to record a signal that provides ample statistical accuracy. The time for the beam to move from one location to the next is short compared to the dwell time, making it appear as a continuous scan. The total time to capture an image frame is given by the product of the total number of points scanned in a field of view and the dwell time at each point. Due to fast scan rates, small discrete points blend into a continuous image composed of various levels of gray produced by differences in signal strength from one location to the other.

Digital imaging technology is efficient and cost-effective and easily lends itself to storage and further handling or processing. Also, several images or frames can be acquired and averaged to reduce noise or charging effects. Additionally, digital images are stored in memory and can be displayed on the screen without having to continuously scan the beam on the specimen surface, thus reducing the probability of beam-induced contamination or damage in sensitive specimens.

In light or transmission electron microscope, rays of light or electrons that originate from a point in an object plane meet at a point in the image plane to form a "true" image. This type of image can be observed directly by placing a viewing screen in the path of the rays. In these techniques, image data is acquired simultaneously from the selected field of view. In the SEM, the image is *enacted* from the signals emitted by the specimen. The image cannot be viewed by placing a screen anywhere in the path of the electrons. The data is collected sequentially in the SEM during the raster scan across the selected field of view. In this context, *true* image is not formed in the SEM.

3.1.2 Relationship Between Picture Element and Pixel

As described in the previous section, the picture element is a discrete location on the specimen where the electron beam dwells and as a result, a signal is generated from that specific location. That signal is processed in the detector and displayed at a corresponding location (called pixel) on the display monitor (see Fig. 3.1). The gray level of that pixel is proportional to the strength of the signal obtained from the corresponding picture element. Since one-to-one correspondence is established between the picture elements on the specimen and the pixels on the screen, it is clear that the number of picture elements will be equal to that of the pixels for a given specimen scan and the resulting image. Let us assume that the digital resolution used for a particular image is 2,000 × 2,000 pixels and the size of the display is 20 × 20 cm. The size (given in horizontal edge length) of one pixel in the image is given as $\frac{20\ \text{cm}}{2,000} = 0.01\ \text{cm} = 100\ \mu\text{m}$. The size of the picture element at the corresponding location of the specimen will be smaller by a magnitude that equals the magnification at which the image was taken. In other words, the length of the picture element can be obtained by dividing the length of the pixel with the value of magnification as shown below:

$$L_{\text{picture element}} = \frac{L_{\text{pixel}}}{M} \tag{3.1}$$

It was stated in Sect. 2.4.6 that the magnification in the SEM is changed by varying the size of the scan on the specimen. The smaller scan produces higher magnification and vice versa. As the size of the scan gets smaller at higher magnification, the size of the picture elements is proportionally reduced to accommodate picture elements whose number is governed by the pixels selected for the image. Conversely, the size of the picture element can be increased by using a smaller magnification during imaging as shown in Table 3.1.

The scattering of the electron beam within the specimen results in an interaction volume much larger than the probe diameter. The signals are generated from a much wider area within the specimen and are not limited to those emanating closer to the probe at the surface. If the diameter of the area that encompasses the scattering within the specimen is projected to the surface and is found to be smaller

Table 3.1 Size of the picture elements at various magnifications for 2,000 × 2,000 pixel image resolution and 20 × 20 cm display size. The pixel size in the image is 100 μm and does not need to be any smaller as the human eye can discern details down to 200 μm only

Magnification	Size of picture element on the specimen, $L_{\text{picture element}}$
10×	10 μm
100×	1 μm
1000×	100 nm
10,000×	10 nm
50,000×	2 nm
100,000×	1 nm
1000,000×	0.1 nm

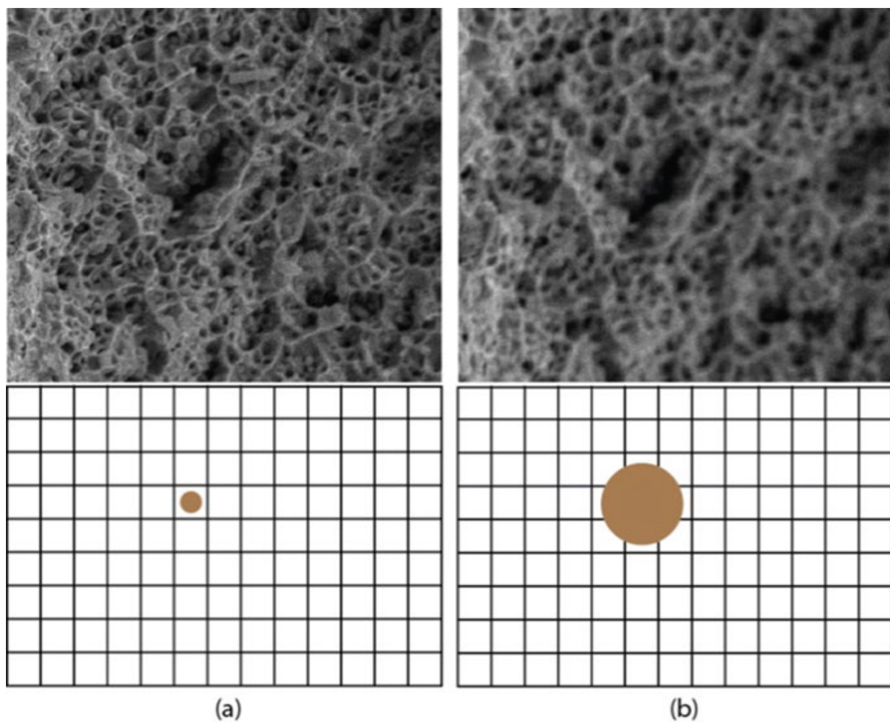

Fig. 3.2 (**a**) If the signal-generating area within the specimen is smaller than the picture element at a particular magnification, the image will appear in sharp focus. (**b**) If the size of the area becomes large, signals from neighboring picture elements will overlap and make the image blur

than the size of the picture element attained at that particular magnification, the image will be in sharp focus. If the probe diameter at the surface or the resulting sampling region within the specimen exceeds the size of the picture element, the image will appear blurred (see Fig. 3.2). The blurring occurs because signals from

adjacent or neighboring picture elements overlap. At high magnifications, the size of picture elements becomes small which readily results in overlap of information and blurring. This directly affects the ability of a microscope to resolve fine details in specimens. The area that produces the signal will vary with the atomic number of material under examination. Light elements will generate large areas, while in heavy elements the signal-generating area within the specimen will be relatively restricted. This has a direct consequence on the ability to produce acceptable images at high magnifications with the same probe diameter. Imaging of light elements at high magnifications is challenging due to greater delocalization of the signal within the specimen.

In summary, the higher is the required magnification the smaller is the pixel size on the specimen surface. If the probe diameter is smaller than the pixel size, the signal produced from the detector might be weak and noisy. On the other hand, if the probe diameter is larger than the pixel size, information from adjacent pixels will be detected, and the sharpness or the resolution of the image will be reduced. Therefore, the optimum probe diameter is comparable to the size of the specimen pixel. This means that in order to achieve optimum performance from an SEM, the spot size should be adjusted according to the magnification of the SEM.

3.1.3 Signal-to-Noise Ratio (SNR)

The interaction between the electron beam and the sample generates a signal that provides useful information about the specimen's topography, structure, or chemistry. The intensity of each pixel in an image is defined by the strength of the signal obtained from the corresponding picture element in the specimen. If the beam is scanned across a single picture element several times, the magnitude of the signal obtained each time will be similar but not exactly identical. Multiple readings of the signal will have an average value, and accompanying variation both below and above that average value will show a Gaussian distribution. The uncertainty associated with the average value of the signal is called noise and is calculated as the standard deviation of the average value of the signal. If the average strength of the signal is n, then the noise is given as $\sqrt{n}$.

Noise is the statistically random variations produced in the signal and is inherent in the process which produces the signal. Noise is part of the signal and increases as the signal gets stronger. Noise also contains fluctuations introduced by amplification and signal processing. Quality of an image is determined by the relative occurrence of signal and noise which is expressed as signal-to-noise ratio (SRN):

$$\mathrm{SNR} = \frac{S}{N} = \frac{n}{\sqrt{n}} = \sqrt{n} \tag{3.2}$$

where $S = n =$ signal and $N = \sqrt{n} =$ noise

When noise increases to an unacceptable level, the image is said to have a low SNR. In order to detect a feature against a background of random noise, signal

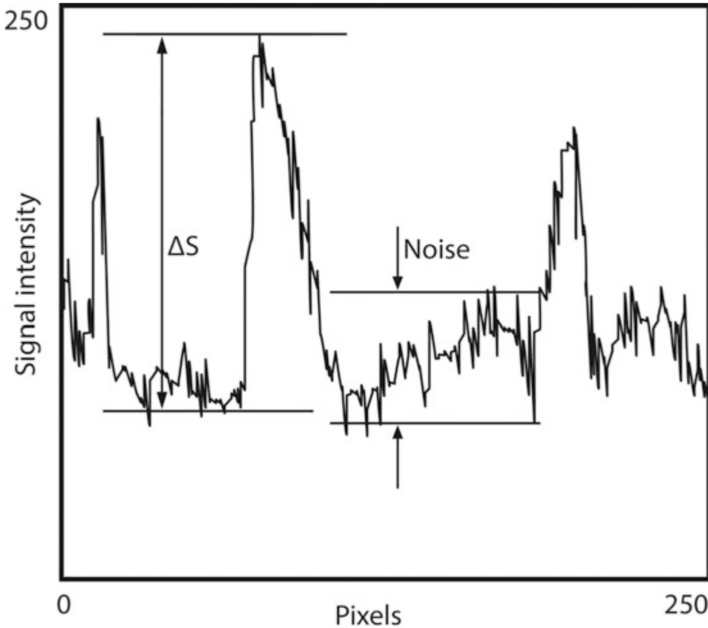

Fig. 3.3 Schematic illustration of statistical fluctuation in a signal giving rise to noise that forms the background of an image. Such a plot is obtained when the beam is scanned on the surface of the specimen once from left to right (called line scan). ΔS is the change in the signal which needs to be roughly $5\times$ of noise to show ample contrast [1]

strength from that feature should be roughly $3\times$ that of the noise level (see the plot in Fig. 3.3) [1]. Signal-to-noise ratio determines the quality of the image. If the SNR is acceptable, the image appears smooth. If the SNR is low, the image looks grainy.

High probe current and slow scan rate set over an optimum range results in high signal-to-noise ratio. As an example, image shown in Fig. 3.4a is taken using small probe current (low SNR) resulting in a grainy image, while that in Fig. 3.4b is taken with large probe current (high SNR) resulting in a smooth image. In another example, the SEM image in Fig. 3.4c was taken at a high scan rate (low SNR) which resulted in a grainy image. The same region appeared smooth (Fig. 3.4d, high SNR) when a small scan rate was used. During a fast scan, the number of probe electrons interacting with each picture element of a specimen is small resulting in a weaker signal emitted that gives rise to low SNR. In practice, the fastest scan rate that gives a smooth image is used in order to prevent charge-up of the specimen which can occur during slow scans. The increased solid angle of collection of the detector will improve SNR. Another way to increase SNR is to take several frames at a high scan rate and undertake frame averaging to reduce the noise. As a post-acquisition procedure, software programs can be used to reduce grainy appearance of an image by *smoothing* operation.

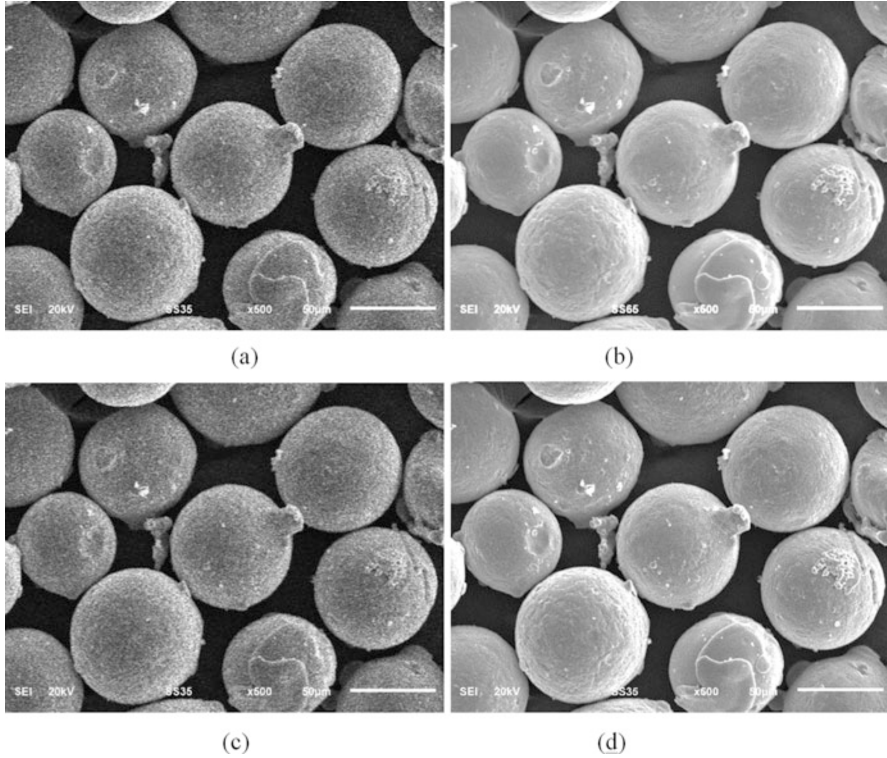

Fig. 3.4 Images of NiCrAlY powder taken under different acquisition conditions: (**a**) small probe current (low SNR), (**b**) large probe current (high SNR), (**c**) high scan rate (low SNR), and (**d**) low scan rate (high SNR). The images depicting high signal-to-noise ratio appear smooth, while those with low SNR show grainy appearance

The SNR of the image is a function of the specimen material, its topography, and the beam current. A filter is needed to remove the noise from the images [2]. For the design of the filter, SNR needs to be estimated. Earliest proposed method involved taking the cross-correlation of two images with the same specimen area [3]. This technique was used by many researchers [4]. However, it requires perfect alignment of the two images, and this method cannot be used for already captured images. The cross-correlation coefficient is given by [5]:

$$\rho_{12} = \frac{r_{12}(0,0) - \mu_1 \mu_2}{\sigma_1 \sigma_2} \tag{3.3}$$

where $r_{12}(0,0)$ is the peak of the cross-correlation function, μ is the image mean, and σ is the variance of the image. The SNR is then calculated as:

$$\text{SNR} = \frac{\rho_{12}}{1 - \rho_{12}} \tag{3.4}$$

Single image method based on autocorrelation was also proposed [6]. This approach involved having the noise be white and adaptive, and to get the noise-free autocorrelation peak function, an estimation technique is used. Two basic techniques were used, the nearest neighborhood (NN) technique and the first-order interpolation (FOI) technique. The autocorrelation coefficient is calculated as:

$$\rho_{12} = \frac{r_{12}(0, 0) - \mu_1^2}{\sigma_1^2} \tag{3.5}$$

Another recent method involves the use of B-spline, cubic spline, statistical autoregressive (AR) model, and mixed Lagrange time delay autoregressive (MLTDEAR) model [5].

Several processes degrade the SNR of an image taken in an SEM, like the secondary emission noise, primary beam noise, and noise from the final detection system. Shot noise in the primary beam arises due to random fluctuation of the number of electrons emitted from the gun. This type of noise is most prominent in thermionic emission guns. The field emission guns are also susceptible to shot noise and flicker noise. The fluctuation in the generation of the secondary electrons emitted per incident beam electron gives rise to secondary electron noise. The detection system that is composed of a photomultiplier tube (PMT) and scintillator contributes to additional noise sources in the SEM image. The noise produced by the detection system is less prominent in comparison to the shot noise and the secondary emission noise [7].

3.1.4 Contrast Formation

Contrast makes a feature in an SEM image distinguishable from other features and the background. It is a measure of visibility of a particular feature in an image. The information contained in a signal emanating from a specimen is interpreted through the formation of contrast. The magnitude of contrast depends on the strength of signals derived from the feature relative to that obtained from its background. The greater the difference in signals, the higher the contrast. Contrast is determined by the difference in the magnitude of signals emitted at two points on the specimen during the beam scan. If the signal from one point is compared with the signal from another point, then the contrast C from the specimen can be written as:

$$C = \frac{S_{\text{A}} - S_{\text{B}}}{S_{\text{A}}} \tag{3.6}$$

where S_A is the signal emitted by the feature A and S_B is the signal emitted by the background. C is always positive (i.e., $S_A > S_B$). Maximum contrast is obtained when S_B equals zero. The contrast level ranges from 0 to 1.

Nature and type of contrast depend on the type of specimen and its interaction with the electron beam and the number of electrons emitted from the specimen based on the operating conditions employed during microscopy. The difference in the signal between the two points may arise due to many factors including change in specimen topography, the difference in composition, crystal orientation, magnetic or electric domains, surface potential, and electrical conductivity. Information about the specimen is contained in the contrast formed by the signals that are emitted from the specimen prior to detection and amplification by the detector. Subsequently, the contrast is modified by the detector without adding new information content. The position and type of detector and its efficiency in collecting and recording the arriving electrons and amplification of the signal play an important role. The strength of the signal collected by the detector depends on the number, energy, and trajectory of electrons, which directly affects the brightness of the pixels in the image.

3.2 Beam-Specimen Interaction

The electrons in the scanning electron microscope are generated by either a thermionic or field emission electron gun. The electrons are transformed into an electron beam by applying a bias voltage that is used to accelerate and focus electrons at a point known as "crossover point." The electron beam then travels in vacuum through electromagnetic lenses, apertures, and scanning coil present within the SEM column to reach the chamber where the specimen to be examined is placed. The electron beam is focused onto the surface of the specimen and scanned across its surface in a raster-like pattern. When an electron beam hits and penetrates a specimen, it is deflected by the specimen in an elastic scattering or inelastic scattering mode. This results in the generation of a variety of signals including secondary electrons, backscattered electrons, Auger electrons, characteristic x-rays, photons, etc. Some of these signals are used to generate SEM images and obtain microchemical information from the specimen. The study of electron beam-specimen interactions that produce such signals is therefore important in order to understand and better control the information obtained from the SEM and also to extract high-quality data using this technique.

3.2.1 Atom Model

The solid specimen to be examined within the SEM is composed of atoms. The nuclei of the atoms, composed of protons and neutrons, are characterized by a concentrated positive charge. The negatively charged electrons are placed around the nucleus in orbits that are grouped together into shells known as K, L, M, etc., as shown in the schematic in Fig. 3.5. The negative charge or energy of the electrons is

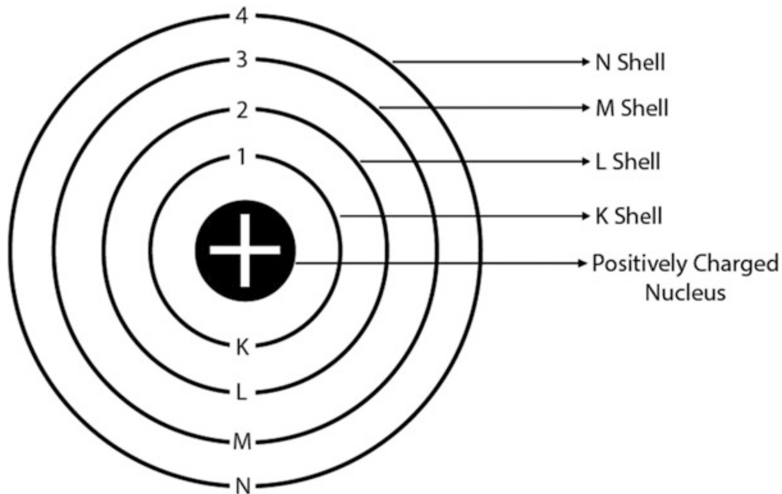

Fig. 3.5 Atom model showing the presence of K, L, M, and N shells at various energy levels around the nucleus

distributed in the way they are placed in orbits. Large atoms or heavy elements contain a larger number of electrons and electron orbits. Each shell contains a large number of energy levels.

3.2.2 Elastic Scattering

The electrons collide and penetrate the specimen surface at an accelerating voltage of 5–20 kV typically used in an SEM. If the electrons are deflected into a new direction by the atomic nuclei without losing any kinetic energy, the mode of beam-specimen interaction is termed as *elastic scattering* as shown in Fig. 3.6.

This deflection of an electron from its original path occurs due to the attractive force exerted on it by a comparatively large positively charged nucleus of the specimen. In this mode of electrostatic interaction with the atomic nuclei, the electrons are deflected at large angles with no significant transfer of energy from the electron to nuclei due to latter's comparatively large mass. The probability of high angle elastic scattering is greater in specimens with heavy/large atoms (roughly proportional to Z^2) due to their stronger positive charge. The tendency of the electron beam to scatter elastically decreases as its energy is increased (proportional to $1/E^2$) since the beam can now more effectively overcome the positive charge of atomic nuclei of the specimen.

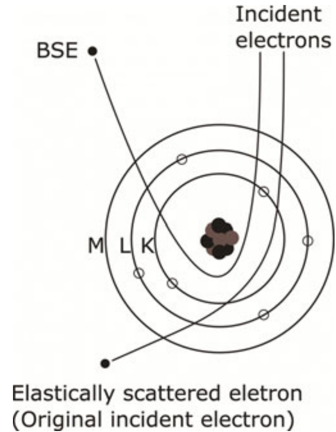

Fig. 3.6 Schematic showing elastic scattering where beam electrons change direction without losing any appreciable energy upon interaction with the Coulombic field of the specimen material

3.2.3 Inelastic Scattering

In addition to elastic scattering, electrons in the electron beam also interact with the specimen in such a way that they lose and transfer their kinetic energy to the atomic nuclei. This type of beam-specimen interaction is known as "inelastic scattering" as shown in Fig. 3.7. Electrons that undergo inelastic scattering are deflected at small angles. The beam electron strikes the electron of an atom in the specimen and knocks it out of its orbit. In the process, beam electron loses energy that is equivalent to that required to create the vacancy in the orbital. Energy dissipation in this type of event is random and gradual and mean energy loss per event is small. The energy of the electrons decreases as a function of distance traveled. Beam electrons keep moving through the specimen lattice till they lose all of their kinetic energy and are brought to rest within the specimen. In metals specimens, they could become conduction electrons. The rate at which these electrons lose energy depends on the density of the specimen and the distance traveled. The higher the density of the specimen material and the greater the distance already traversed by the beam within the material, the greater the energy loss. The rate of energy loss is defined by the "stopping power" S of the target material as shown in the following equation:

$$S = -\left(\frac{1}{\rho}\right)\frac{dE_0}{ds} \tag{3.7}$$

where ρ is the density of the specimen material

E_0 is the incidence beam energy

s is the distance traveled by the electron within the specimen

S is the rate of energy loss divided by the target density. Loss of energy is denoted by the negative sign. The electron energy is reduced approximately by 1–10 eV per nanometer of distance traveled within the specimen depending on its atomic number. For every unit of length (i.e., nm) traveled, beam electrons will lose more energy in heavy elements than in light elements. However, for every unit

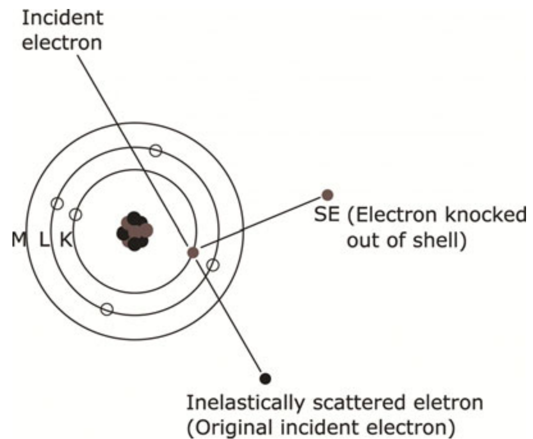

Fig. 3.7 Schematic diagram showing inelastic scattering where beam electron knocks out an orbital electron belonging to the specimen losing energy in the process

of mass (i.e., gram), light elements will extract more energy compared to heavy elements. This is due to the fact that light elements have a higher number of electrons per unit mass compared to heavy elements. This larger number of specimen electrons will give rise to a greater number of inelastic scattering events making the beam electrons lose energy more rapidly.

3.2.4 Effect of Electron Scattering

It is clear from above that when electron beam hits the specimen, the electrons do not remain confined at the surface of the specimen within a region where the electrons are converged, nor do they penetrate into the specimen in a straight line. On the contrary, elastic and inelastic scattering events make them penetrate into the depth and spread laterally across the width of the specimen forming a relatively large *interaction volume*. The density of elastic scattering events changes from the point of beam impact to the boundary of the interaction volume. It is important to realize that this is the volume of the specimen where from all imaging and the microchemical information is extracted. For instance, when an electron beam with an energy of 20 keV is converged onto the specimen surface to a very small probe diameter of few nanometers, it can penetrate 5 microns and spread 1 micron into the specimen depending on latter's density (as shown in Fig. 3.8). Therefore, the information obtained from the specimen is not restricted to the diameter of the incident probe but is gathered from a volume that is larger by hundreds to thousand times of the beam size. Due to electron scattering, the signal is generated from a large area of the specimen, thus restricting the spatial and analytical resolution of the SEM.

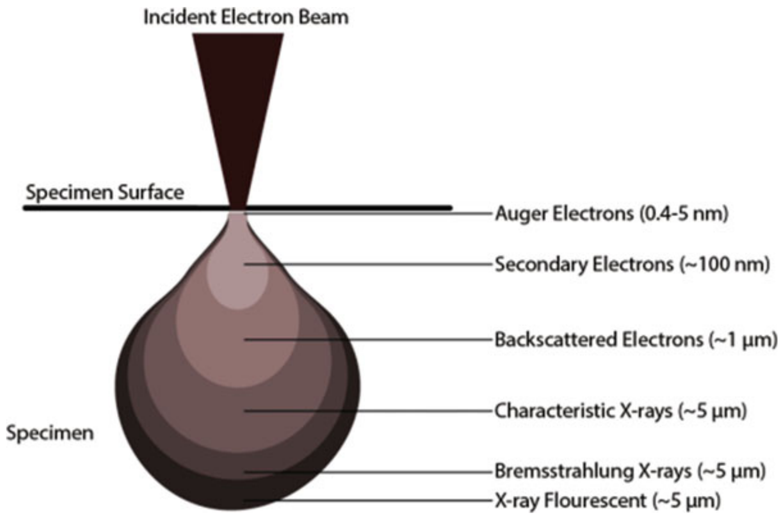

Fig. 3.8 Schematic illustrating the formation of *teardrop* interaction volume upon scattering of the electron beam within the specimen. The probe diameter of a few nanometers results in several cubic micrometers of volume where from signals are generated. This limits the spatial and analytical resolution of the SEM

3.2.5 Interaction Volume

The total volume of the specimen material that is affected by the incident electron beam is known as the interaction volume and is much larger compared to the size of the incident probe. The size of the interaction volume created depends on the specimen density, beam energy, and probe current density. Interaction volume represents the averaged behavior of a large number of electrons. Monte Carlo method is a computer simulation of electron trajectories within a specimen and aids in investigating the interaction volume created in a specific material under given beam conditions. This kind of simulation treats scattering as a statistical process and gives a visual perspective to the spatial distribution of electron scattering process. It depicts the volume of material from where various signals are collected. The simulation provides *first principles* approach using various models that take into account the collective effect of elastic and inelastic scattering to determine electron paths, deflection angles, and energy loss. The electron is treated as a discrete particle and the specimen material is taken as amorphous. Spatial distribution of secondary and backscattered electrons, as well as x-rays, can be obtained using this method [1, 8, 9].

3.2.5.1 Effect of Beam Energy on Interaction Volume

Monte Carlo electron trajectory simulations as a function of electron beam energy (E_0) in various elements are shown in Fig. 3.9. The higher the beam energy, the greater the depth and width to which the electrons can travel into the specimen as

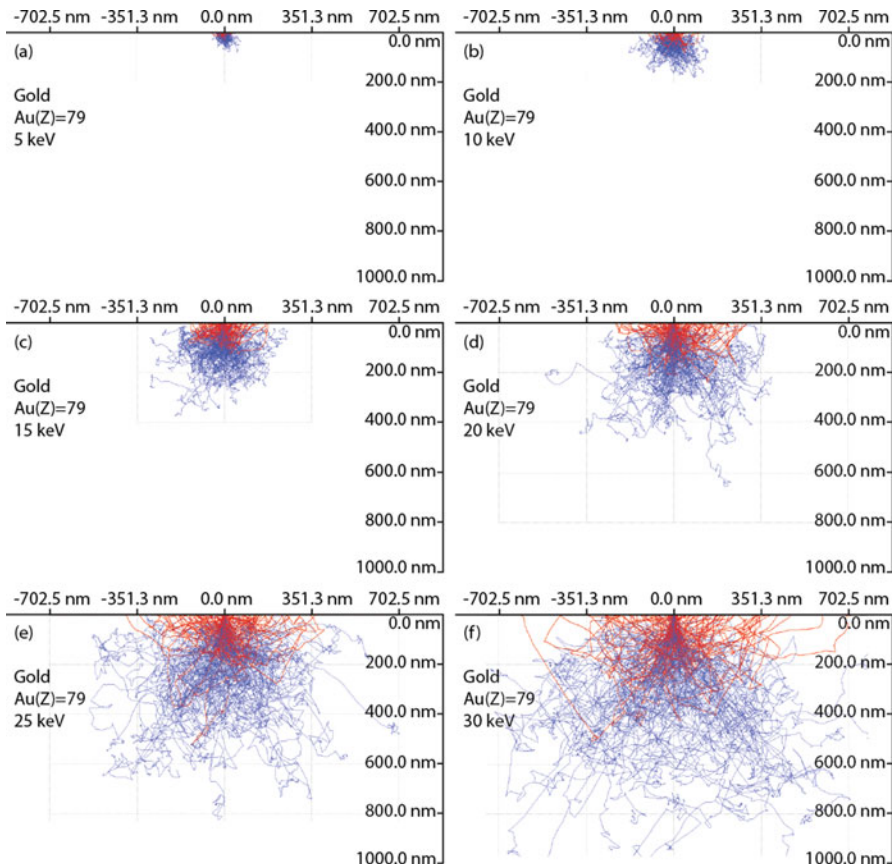

Fig. 3.9 Monte Carlo simulations showing the extent of interaction volume formed in a specimen of Au. From beam energies of 5–30 keV, depth of beam penetration increases from 60 nm to 1000 nm and width from 100 nm to 1400 nm. Note that the shape of the interaction volume does not change with beam energy

they lose energy at a lower rate which is proportional to $\frac{1}{E_0}$. Increasing beam energy also reduces its probability to scatter elastically (as a function of $\frac{1}{E_0^2}$), thus penetrating deeper into the specimen. The trajectories of the electrons near the specimen surface are straight resulting in widening of the interaction volume away from the surface.

3.2.5.2 Effect of Atomic Number on Interaction Volume

For specimens with a high atomic number, the elastic scattering is greater resulting in a deviation of the electrons from their original path more quickly and reducing the distance that they travel into the specimen as shown in Fig. 3.10a–e. The widening of the interaction volume is caused closer to the specimen surface as the probability of

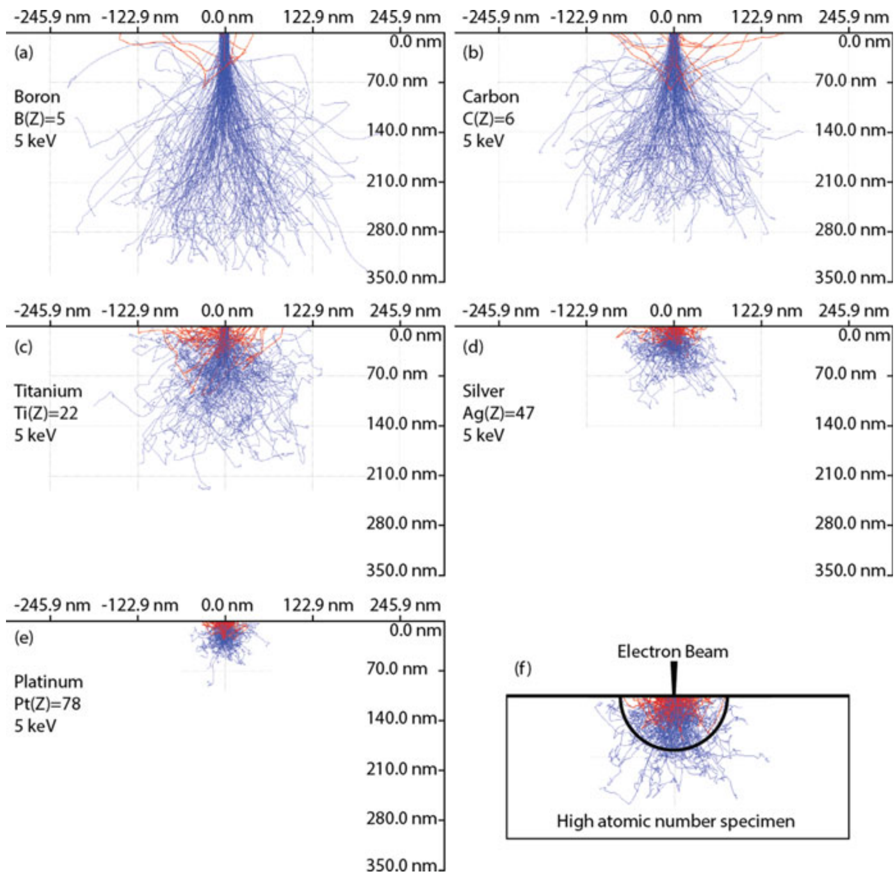

Fig. 3.10 (**a**–**e**) Monte Carlo simulations showing the extent of interaction volume formed within various elements at 5 keV. Depth and width of beam spread are the greatest in B ($Z = 5$) and lowest in Pt ($Z = 78$). The shape of interaction volume is considerably different for elements of low and high atomic numbers. In the elements of low Z, beam penetrates deeper before it deviates and spreads across. For elements with high Z, beam tends to deviate from its original path more quickly resulting in delocalization closer to the surface of the specimen. (**f**) Schematic representation of hemispherical interaction volume typically formed in the elements of high atomic number

elastic scattering as well as its angle increases in an element of high Z. Also, the rate of energy loss for electrons is high in the linear dimension resulting in a relatively shallow interaction volume within a high atomic number specimen. This phenomenon results in a hemispherical shape of the interaction volume (see schematic diagram in Fig. 3.10f). On the other hand, elastic scattering and the rate of energy loss per unit length are lower in low atomic number targets due to which beam electrons manage to maintain their straight trajectories for larger depths in the specimen. This results in the formation of a large interaction volume taking the form of a *teardrop* (as shown in Fig. 3.8).

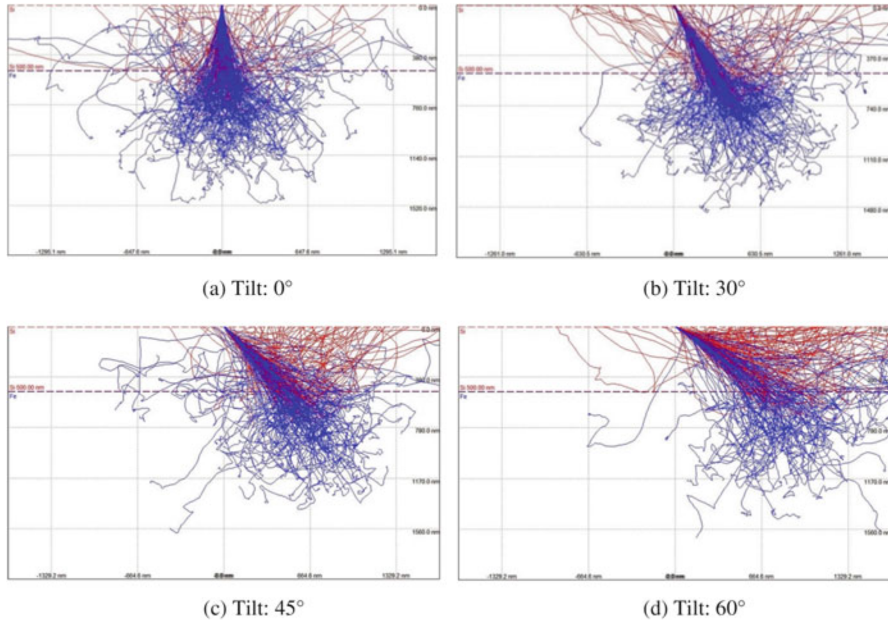

(a) Tilt: 0° (b) Tilt: 30°

(c) Tilt: 45° (d) Tilt: 60°

Fig. 3.11 (**a**–**d**) Monte Carlo simulations of electron trajectories showing the extent of interaction volume formed at various tilt angles of the electron beam. As tilt angle is increased, a large part of the interaction volume is generated close to the specimen surface which allows a larger number of electrons to escape the specimen. This also results in an asymmetry in the shape of the interaction volume

3.2.5.3 Effect of Tilt on Interaction Volume

Interaction volume also changes with the tilt of the specimen with respect to the beam. It is the maximum when the specimen is inclined 90° with respect to the beam. As the angle of inclination between the beam and specimen is narrowed, a greater number of electrons can escape the specimen surface which when tilted lies closer to the forward scattering direction (i.e., less than 90°) of electrons. This can be understood by visualizing part of the interaction volume lying outside the specimen surface, as shown in Fig. 3.11.

3.2.6 Electron Range

Electron range (or penetration depth) describes complex three-dimensional interaction volume in simple terms and can be used to provide quick rough comparisons between various materials. It is defined as the mean straight line distance of the electron from the point of entry to point of final rest in the specimen. A hemisphere is formed with a radius whose origin is at the point of beam penetration, and it contains 90–95% of the scattered electrons (see Fig. 3.12). The radius of this hemisphere is taken as the electron range given in microns as shown in the following expression [10]:

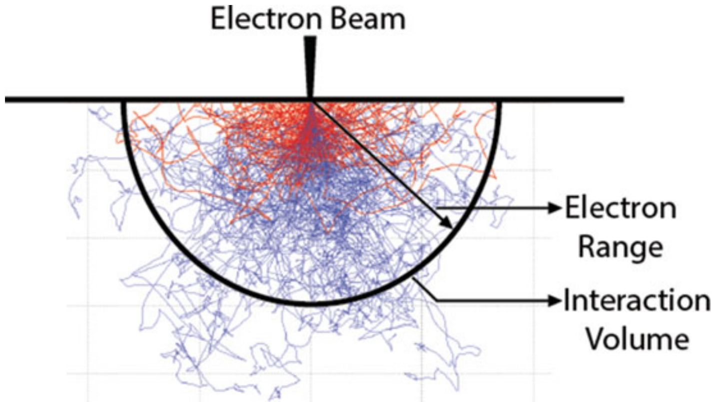

Fig. 3.12 Schematic representation of electron range (*R*) or penetration depth by drawing a hemisphere from the point of beam penetration that covers most of the scattered electrons

$$R = \frac{0.0276\, AE_0^{1.67}}{\rho Z^{0.89}} \tag{3.8}$$

where

R = electron range, μm
A = atomic weight, g/mole
E_0 = beam energy, keV
ρ = density, g/cm^3
Z = atomic number

This equation can be used for specimens that are considered bulk (thick), large (free of edges or boundaries), and flat. It can be seen from Eq. 3.8 that electron range or penetration depth decreases substantially at low beam energy as fewer collisions are required to bring the low-energy electrons to a stop. Additionally, the probability of inelastic scattering increases with decreasing beam energy (i.e., it is proportional to $\frac{1}{E_0}$). This results in smaller interaction volume at low beam energy. This is especially true for elements with low *Z*. For example, for C, Al_2O_3, and SiO_2, when the beam energy is lowered from 15 to 1 keV, the interaction volume is reduced by 5–6 orders of magnitude, and the electron range is decreased by 2 orders of magnitude. For high-*Z* elements, the decrease is not as severe.

For a given beam energy, the penetration depth is primarily influenced by and inversely proportional to the atomic number (and density) of specimen material. It is clear from Eq. 3.8 that the penetration depth becomes smaller as *Z* increases. For example at 10 keV, the beam penetrates roughly 1 μm in C while only 0.2 μm in Au. In elements of high atomic number, a large number of electrons are elastically scattered at high angles deviating them from straight trajectories resulting in small *R*. As a consequence, the interaction volume is smaller in elements of high *Z*.

Electron range can be expressed in terms of mass thickness making it independent of Z as follows:

$$\rho R = aE_0^b \quad (3.9) \quad [11]$$

where ρ is the density, R is the electron range, E_0 is the beam energy, a is approximately 10 μg/cm^2, and b varies between 1.33 (at low E_0) and 1.67 (at high E_0).

Electron range of a tilted specimen decreases as the interaction volume becomes asymmetric and allows a large number of electrons to escape. Value of R will depend on the angle of tilt and can be given as:

$$R(\theta) = R(0)\cos\theta \quad (3.10)$$

where $R(0)$ is calculated at 0° tilt

3.3 Origin of Backscattered and Secondary Electrons

3.3.1 Origin of Backscattered Electrons (BSE)

As discussed in the previous sections, beam electrons undergo multiple elastic and inelastic scattering events giving rise to a large region within the specimen called interaction volume. The extent of each type of scattering depends on the beam energy, atomic number of the target and the degree of tilt used. Elastically scattered beam electrons are deflected through large angles (>90°) and eventually find their way out of the specimen giving rise to the phenomenon of *backscattering*. These electrons are called *backscattered electrons* (BSE), and they originally belong to the incident electron beam that strikes the surface of the specimen. The surface of entrance and departure may or may not be the same. Backscattered electrons make up most of the electron signal emanating from the specimen. These electrons constitute a significant proportion of the total energy of the incident beam. With the escape of BSE from the specimen, a substantial measure of beam energy is removed from the sample. Once out in the vacuum, these electrons can be captured by a detector and used to form an image called *backscattered electron image*. The contrast exhibited by the image formed due to these electrons is called *compositional* or *atomic number* (Z) *contrast*.

3.3.2 Origin of Secondary Electrons (SE)

In addition to BSE, some electrons belonging to the target material are also ejected from the specimen. These electrons are generally loosely bound outer shell electrons residing close to the specimen surface and are struck by the electrons of the incident beam in an inelastic manner. Outer shell electrons are knocked out of their shells. If adequate energy is imparted to them in the process, they may find their way out of the specimen due to their close proximity to the surface. These

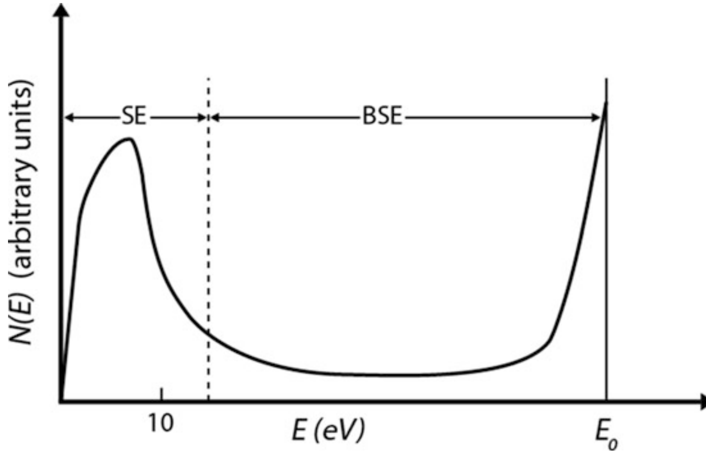

Fig. 3.13 Schematic representation of electron energy distribution where $N(E)$ is the number of electrons of energy E emitted by a specimen irradiated with incident electrons of energy E_0. Backscattered electrons dominate the energy spectrum, while low-energy secondary electrons are generated in small numbers

electrons that originally belong to the specimen material and are ejected out of the specimen are known as *secondary electrons* (SE). These can be collected by a detector to form a secondary electron image. The contrast exhibited by SE is known as *topographic contrast*.

An electron is an electron and as such, no distinction between secondary and backscattered electrons can be made. They are differentiated purely on the basis of their energy, i.e., electrons that are emitted from the specimen with less than 50 eV kinetic energy are classified as secondary electrons.

The plot in Fig. 3.13 shows the distribution of energy of all electrons that emanate from a specimen. The y-axis shows the number of ejected electrons $N\ (E)$, and the x-axis represents the energy of electrons emanating from specimen starting from zero to the primary beam energy incident on the specimen surface (E_0). The region to the far right of the plot represents electrons that are ejected from the specimen with no loss of energy. In addition, the greater part of the energy spectrum corresponds to electrons that are ejected from the specimen with relatively high energy. These are called backscattered electrons. The number of low-energy backscattered electrons emanating from the specimen falls close to zero as the left-hand side of the plot is approached. Beyond this point, an abrupt increase is observed in the number of electrons that emanate from the specimen. These electrons have energies of 50 eV or less at energy scale. This sudden increase in the number of electrons with low energy is attributed to the generation of secondary electrons.

3.4 Types of Contrast

Compositional and topographic contrasts are the two dominant forms of contrast used in scanning electron microscopy. These are primarily dependent on backscattered and secondary electrons which make up the most important signals used in SEM imaging. It is important to study the dependence of these signals on beam energy, atomic number, tilt, and other related factors. Most images depict a combination of contrast mechanisms. Discussion of each contrast mechanism and its applications follows in the proceeding sections.

3.4.1 Compositional or Atomic Number (*Z*) Contrast (Backscattered Electron Imaging)

3.4.1.1 Yield of Backscattered Electrons

The extent of backscattering in a specimen is expressed in the form of backscatter coefficient (η) which is defined as the fraction of incident electrons that leave the specimen surface, as shown below:

$$\eta = \frac{\eta_{\mathrm{BSE}}}{\eta_{\mathrm{B}}} \tag{3.11}$$

where

η = backscatter coefficient

η_{BSE} = number of backscattered electrons

η_{B} = number of incident beam electrons

The backscatter coefficient can be measured in terms of the ratio of backscattered current moving out of the specimen to that of the incident beam current.

$$\eta = \frac{i_{\mathrm{BSE}}}{i_{\mathrm{B}}} \tag{3.12}$$

where

η = backscatter coefficient

i_{BSE} = backscattered electron current moving out of the specimen

i_{B} = electron beam current entering the specimen

Elastic scattering occurs mostly in the forward direction that involves deflections at small angles (e.g., 5°). The incident beam tends to penetrate into the specimen in roughly the same direction it entered. Backscattering occurs only as a cumulative effect of numerous small- and some large-angle scattering events. This results in electrons changing direction to the extent that they escape as backscattered electrons from the surface they initially entered.

3.4.1.2 Energy Distribution of BSE Yield

Some beam electrons will enter the specimen, immediately deflect through large angles, and leave the specimen without any energy loss. The energy of these

backscattered electrons will be equal to the energy of the incident beam. Other beam electrons will travel through the specimen until they lose almost all of their energy prior to ejecting out of specimen surface. These BSE will have essentially zero energy upon exclusion. The energy continuum of backscattered electrons, therefore, stretches from zero to incident beam energy E_0. By convention, the energy of the BSE is generally defined as 50 eV < $E_{BSE} \leq E_0$. Electrons with <50 eV energy are classified as secondary electrons. Majority of BSE emanating out of specimen undergo multiple scattering events within the specimen. Most of the backscattered electrons retain at least 50% of their energy at the time of ejection from the specimen.

In specimens with intermediate to high atomic numbers, the majority of backscattered electrons will have higher energy distribution. This is due to the fact that the degree of elastic scattering and hence backscattering increases with atomic number. On the other hand, lesser number of backscattered electrons emanating from a specimen with low atomic number will depict high energy. It can be seen in Fig. 3.13 that a broad region toward the left of the E_0 peak is covered by BSE. For elements with high Z, the majority of the BSE ejected from the specimen will exhibit energies of the order of $\geq 0.7E_0$. For the elements with low Z, the BSE energy is $\geq 0.4E_0$. Heavy elements such as Au can exhibit significant BSE yield with energy $0.9E_0$, whereas the equivalent for a light element such as C is at $(0.5–0.6)E_0$. Half of the BSE yield from Au and C will have energy of $0.84E_0$ and $0.55E_0$, respectively.

The strength of the signal output from the detector depends not only on the number of BSE but also on their energy. The contrast produced in the image, therefore, is a combination of mean Z of the specimen and the energy distribution of BSE ejected from it. Combination of high mean Z and high-energy distribution of BSE imparts a strong contrast to the BSE image of specimens with high density.

3.4.1.3 Effect of Beam Energy on BSE Yield

Backscattered electrons are generated from a depth that is roughly one-third of the penetration depth of the incident beam or electron range. The size of interaction volume formed in a given target material increases with an increase in beam energy. The electrons with high energy travel deep into the specimen. Although these electrons penetrate deeper, they still have enough energy to get deflected at large angles and leave the specimen surface. Therefore, the backscatter coefficient changes only slightly (<10%) at incident electron beam energy of 10, 20, and 30 keV as seen in Fig. 3.14a. At lower beam energy of <5 keV, backscatter coefficient increases for elements with $Z < 30$ and decreases for elements with $Z > 30$. This complicates the BSE contrast formed at low beam energies and interpretation of images needs careful consideration.

3.4.1.4 Effect of Atomic Number on BSE Yield

Backscatter coefficient η strongly depends on the atomic number of the specimen material. Target materials with high atomic number show a high degree of elastic scattering resulting in high angles of deflection and large backscattering effect. The relationship between backscattered coefficient η and atomic number Z is plotted for 10–30 keV incident beams in Fig. 3.14a.

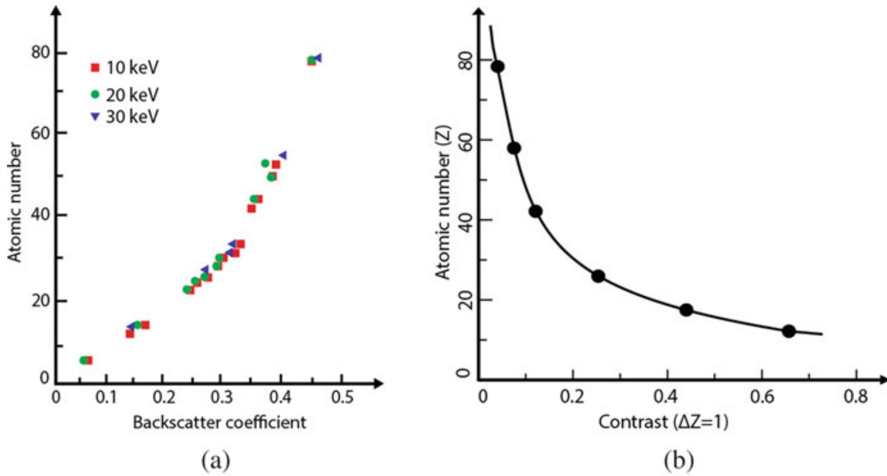

Fig. 3.14 (**a**) Backscatter coefficient η increases with atomic number Z. This behavior is similar at various beam energies (10–30 keV plotted in the graph). Backscatter yield is <10% for light elements and increases to around 50% for heavy elements. (**b**) Curve fit to the adjacent plot reveals atomic number contrast from a pair of elements that are one atomic number apart

It can be seen from the plot that the backscatter coefficient increases with atomic number. Backscatter yield is approx. 10% for light elements and increases to >50% for heavy elements. It immediately follows that two phases with different atomic numbers present within a specimen will exhibit different values of backscatter coefficient. This will result in a contrast where the phase with a high atomic number will appear relatively brighter (due to a larger number of backscatter electrons ejecting out of this phase) while phase with a low atomic number will appear relatively dark. This is called compositional or atomic number or Z contrast. It follows from the above discussion that the contrast of the phases in BSE images will depend on their chemical composition. The phases with strong contrast (i.e., appearing bright) contain heavier elements (higher Z), and the phases with weak contrast (i.e., appearing dark) constitute lighter elements (lower Z). It can be seen in Fig. 3.14a that the contrast produced between elements with a large difference in atomic numbers will be strong. For example, the contrast generated between Al ($Z = 13$) and Au ($Z = 79$) is 69% while that between Al ($Z = 13$) and Si ($Z = 14$) is mere 6.7%. It can also be seen in Fig. 3.14a that the slope is initially steep and then declines gradually beyond atomic number 40. This means that Z contrast is stronger between two low atomic number phases compared to two high atomic number phases. This relationship is expressed in a plot in Fig. 3.14b which shows decreasing contrast with increasing Z between two successive elements in the periodic table. As an example, the contrast between light B ($Z = 5$) and C ($Z = 6$) is 14% while the contrast between heavy Pt ($Z = 78$) and Au ($Z = 79$) is 0.41% only. Any contrast $\geq$10% is easily discernible in the SEM. The contrast between 1% and 10% requires effort to image, while the contrast of <1% is difficult to detect. Weak Z contrast formed between two phases with similar density requires the use of well-polished flat

specimens to increase the BSE collection efficiency. In addition, use of short working distance and large detector surface area also increases the signal-to-noise ratio.

Backscattering coefficient increases and approaches unity for all elements as the specimen is tilted. So, the differences in η between elements decrease in turn diminishing the contrast formed at high tilt angles. Backscattering coefficient for an element can be calculated using the following empirical equation [12, 13]:

$$\eta = -0.0254 + 0.016Z - 1.86 \times 10^{-4}Z^2 + 8.3 \times 10^{-7}Z^3 \tag{3.13}$$

When a target is a homogeneous mixture of elements at an atomic scale, a simple rule of mixtures can be used:

$$\eta = \sum_i C_i \eta_i \tag{3.14}$$

where

i is an individual element

C_i is the mass fraction of element i

η_i is backscatter coefficient of element i

In addition to qualitatively identifying chemically distinct phases, Fig. 3.14a can be used to obtain quantitative chemical information from a phase. This is undertaken by measuring the BSE signal emitted from a phase, comparing it with the signal intensity from a known pure elemental standard and using the plot in Fig. 3.14a to determine the atomic number of the phase. This technique can be used to detect phases with low Z. The detected BSE signal should not contain a contribution from topography or crystallographic contrast.

A typical backscattered image of the fracture surface of an Al alloy depicting Z contrast is shown in Fig. 3.15.

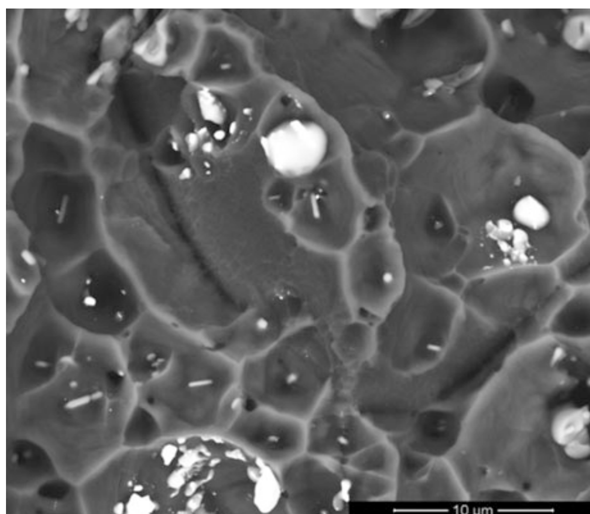

Fig. 3.15 Backscattered electron image of the fracture surface of an Al alloy showing the presence of coarse precipitates. Compositional or Z contrast makes the precipitates appear brighter indicating that they are composed of heavy elements compared to the surrounding matrix of Al alloy

3.4.1.5 Effect of Tilt on BSE Yield

Tilt angle θ is defined as the complement of the angle between the beam and the specimen surface. Backscatter coefficient changes with the degree of tilt of the specimen with respect to the beam. It is the minimum when the specimen is placed 90° with respect to the beam (tilt angle $\theta = 0°$). As the angle of inclination between the beam and specimen is narrowed (as θ increases), a greater number of electrons can escape the specimen surface as backscattered electrons. The surface of the specimen when tilted lies closer to the forward scattering direction of electrons. This means that backscattered signal from the specimen can be increased by tilting the specimen in such a way that the incidence angle of the beam with the specimen surface is small, i.e., θ is large. A monotonic increase in backscatter coefficient η with tilt angle θ can be expressed by the following equation:

$$\eta(\theta) = (1 + \cos\theta)^{\frac{-9}{\sqrt{z}}} \tag{3.15}$$

This is depicted in a plot obtained from a specimen of Fe coated with a thin (200 nm) film of Zr as shown in Fig. 3.16a. The figure also shows Monte Carlo simulations of electron trajectories for the same specimen tilted at various angles θ of (b) 0°, (c) 20°, (d) 60°, and (e) 70°. It can be seen that the interaction volume becomes increasingly asymmetric with increasing θ resulting in an increase of backscatter coefficient. It is also important to note that the energy distribution of BSE is shifted toward higher energy at high tilt angles, especially if $\theta \geq 70°$.

3.4.1.6 Effect of Crystal Structure on BSE Yield

The backscatter coefficient η is marginally sensitive to the direction of the incidence beam relative to the crystal lattice in a single-crystal specimen. If the beam penetrates along the direction of the densely packed atomic planes, the η is higher. The backscatter coefficient will be lower if the beam direction is along the low-density planes which allow the beam to penetrate deeper into the specimen before scattering, thus resulting in a lower η. The variation in η due to crystal structure is however low (i.e., in the order of 1–10% maximum). The difference in η due to crystal orientation forms the basis for *electron channeling contrast*.

3.4.1.7 Directional Dependence of BSE Yield

Upon interaction of the electron beam with the specimen, the backscattered electrons are emitted in all directions and follow straight trajectories. They follow the direction toward which they were initially ejected. However, the number of emitted BSE and hence their intensity is not the same in all directions. BSE angular distribution will follow a cosine law. Due to this reason, the collection efficiency of the detector receiving these electrons will depend on the detector's position within the specimen chamber. At zero-degree specimen tilt ($\theta = 0°$, beam normal to the specimen surface), the maximum number of backscattered electrons is emitted along the beam, i.e., normal n to the specimen surface (see Fig. 3.17). Backscatter coefficient η will be the highest along the beam direction as BSE are predominantly emitted back toward that point. At location m which is at an angle $\varnothing$ relative to the normal n, the number of emitted BSE will decrease and is given by:

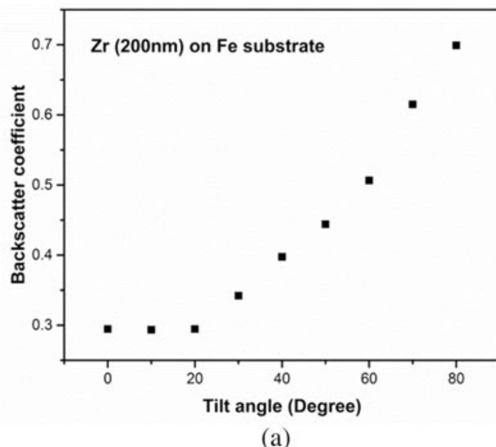

(a)

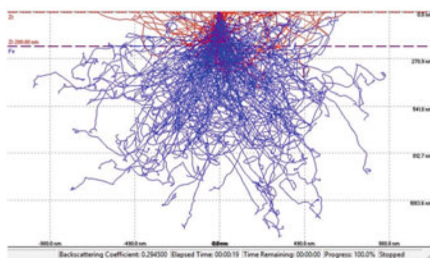

(b) θ = 0

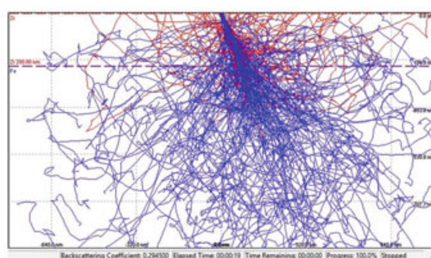

(c) θ = 20°

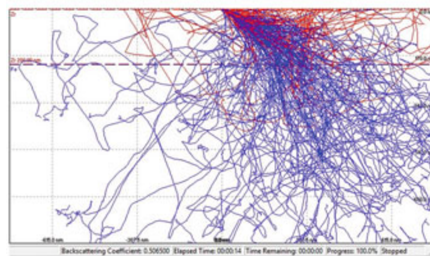

(d) θ = 60°

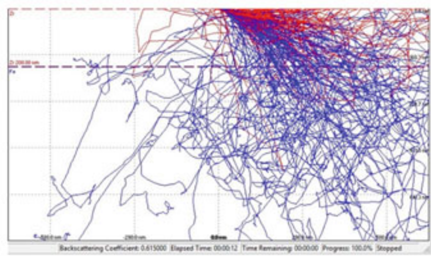

(e) θ = 70°

Fig. 3.16 Specimen: Fe coated with Zr. (**a**) Plot showing typical increase in backscatter coefficient as the tilt angle θ (defined as the complement of the angle between the beam and the specimen) is increased. As the incidence angle of the beam with the specimen surface is narrowed (θ is increased), a large proportion of elastically scattered electrons are able to escape the surface as the interaction volume intersects the latter. The figure also shows Monte Carlo simulations of electron trajectories at various tilt angles θ of (**b**) 0°, (**c**) 20°, (**d**) 60°, and (**e**) 70°. It can be seen that interaction volume becomes increasingly asymmetric with increasing θ resulting in an increase in backscattering [14]

Fig. 3.17 At zero specimen tilt ($\theta = 0°$), backscatter coefficient η is the highest along normal n to the specimen surface (i.e., at $\varnothing = 0$). As the value of $\varnothing$ increases, η will decrease. At $\varnothing = 45°$, η is 71% of that at n. At $\varnothing = 75°$, η is reduced to 26% of that at n

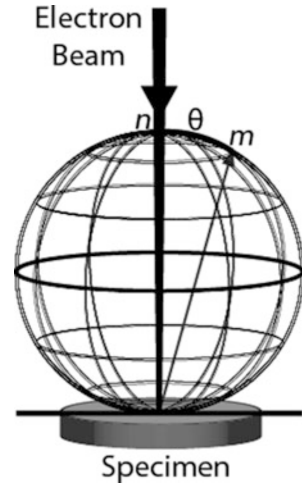

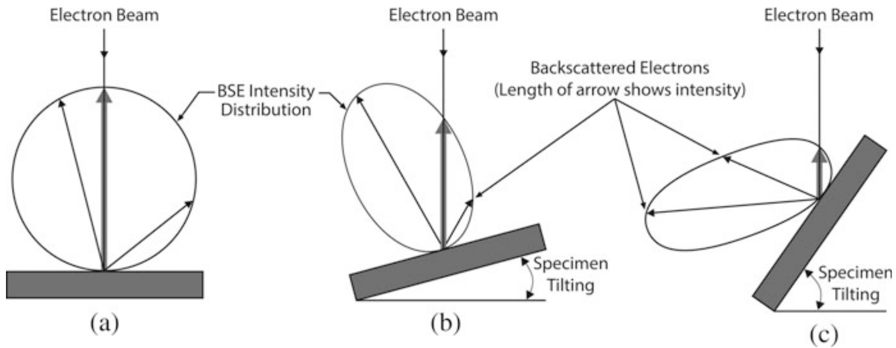

Fig. 3.18 (**a**) The circle represents the magnitude of backscatter coefficient η at various angles of BSE generation. Vector length within the circle corresponds to the magnitude of η at a particular angle. Large vector at a high angle of emission relative to the specimen surface indicates higher η. Small vector at a shallow angle of emission represents lower η. (**b**, **c**) As the specimen is tilted, the emission pattern changes into an elliptical shape where the highest emission corresponds to the longest vector of the asymmetric ellipse

$$\eta_m = \eta_n \cos \varnothing \tag{3.16}$$

where

η_m= backscatter coefficient at m

η_n = backscatter coefficient at n

In Fig. 3.18a, the circle represents the magnitude of BSE intensity at various angles of emission, while lengths of the vectors drawn within the circle indicate the magnitude of BSE intensity at a particular angle. At zero-degree specimen tilt, the largest vector is obtained along the beam direction indicating maximum emission in

this direction. The vector length becomes small at shallow angles relative to the specimen surface indicating smaller η. As the specimen is tilted, the circle that represents BSE intensity begins to change its shape into an ellipse. Largest vector does not correspond to the beam direction at this stage (see Fig. 3.18b). As the degree of tilt is further increased, the ellipse becomes more asymmetric with the largest vector now lying at increasingly shallow angles relative to the specimen surface (see Fig. 3.18c). This occurs because the interaction volume begins to intersect the specimen surface and more and more backscattering occurs from this surface due to the tendency of electrons to scatter in the forward direction. Maximum BSE generation will now occur along the long axis of the asymmetric ellipse and not in the direction normal to the specimen surface.

3.4.1.8 Collection Efficiency of the BSE Detector

It follows from above that the collection efficiency of the BSE detector depends on its location. If a detector is placed directly above and normal to the non-tilted specimen surface (i.e., at *n* in Fig. 3.17), it will have the highest collection efficiency. The BSE collection efficiency of a detector placed at location *m* will be reduced compared to that located at *n* (Fig. 3.17). This is also shown schematically in Fig. 3.19a. For non-tilted specimen, collection efficiency is reduced if the detector is placed at narrow angles relative to the specimen surface. In this case, collection efficiency can be improved by tilting the specimen toward the detector as shown in Fig. 3.19b. Once the specimen is tilted, the circle that represents BSE intensity changes to an elliptical shape especially at high tilt angles. Maximum BSE generation will occur along the long axis of the asymmetric ellipse and not in the direction normal to the specimen surface as shown in Fig. 3.19b. It can be concluded that for a detector that is located above the specimen, maximum collection efficiency for BSE

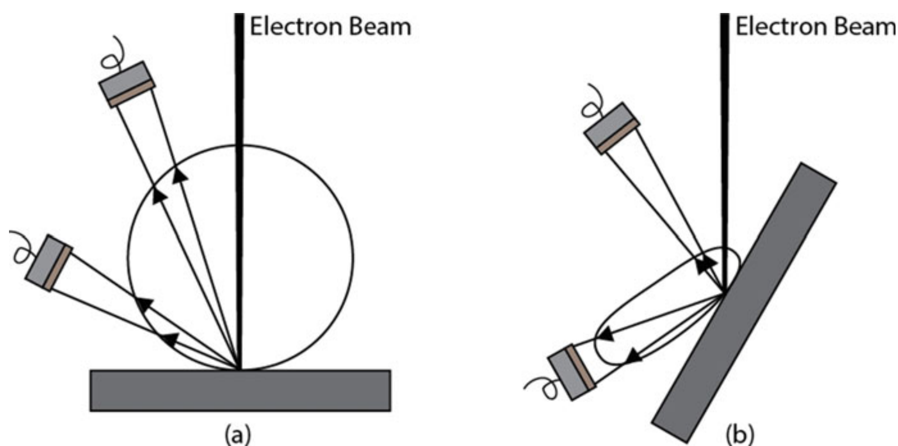

Fig. 3.19 In case of (**a**) where beam incidence is normal to the specimen surface, the maximum collection efficiency is obtained by placing the detector directly above the specimen. In case of (**b**) where the detector is placed at a small angle relative to the specimen surface, the maximum collection is obtained by tilting the specimen toward the detector

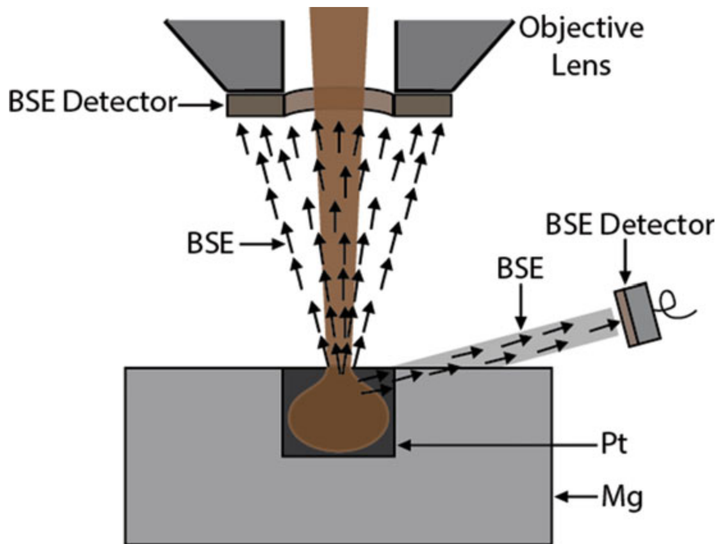

Fig. 3.20 Detector placed at a shallow angle will form an image with BSE that emanate from Pt particle and travel through Mg matrix resulting in blurring of the Pt edge that faces the detector

is obtained by keeping the specimen at zero tilt. For a detector that is placed at a small angle relative to the specimen surface, maximum collection efficiency for BSE is obtained by tilting the specimen toward the detector.

The detector placed at a shallow angle will not only receive the weaker backscattered signal but also form an image with BSE that travel a large distance through the material before they are ejected out of the specimen. This tends to degrade image resolution, especially in a multiphase material. Consider a case where the specimen constitutes of the high-Z particle (e.g., Pt) dispersed in a low-Z matrix (e.g., Mg) as shown schematically in Fig. 3.20. The BSE emanating from Pt have to pass through Mg before they are ejected and enter into the BSE detector placed at a small angle relative to the specimen surface. As a result, the edge of the Pt particle closer to the detector will lose sharpness and appear blurred in the image.

3.4.1.9 Spatial Distribution of BSE

As the atomic number of the target material increases, the depth and lateral dimensions from which the BSE signal is emanated decrease. For example, at a beam energy of 30 keV, the escape depth of BSE in Al and Au is 2.3 μm and 0.45 μm, respectively. Similarly, the lateral dimension from which the BSE signal is derived in Al and Au is 10.6 μm and 1.3 μm, respectively. The depth within the electron range from which BSE is derived depends on the atomic number of the target material. For instance, 95% of BSE are ejected from 19% of the penetration depth in Au while 95% of BSE are derived from 32% of penetration depth in C.

The depth and lateral dimensions of the volume that emit BSE signal increase with increasing incidence beam energy E_0. The BSE signal is generated from a

substantial depth of the electron range at a beam energy of $\geq$10 keV. Due to this fact, any hidden subsurface features (e.g., voids, inclusions, second phase particles, etc.) with different atomic numbers or density than the surface material can be detected due to a difference in the magnitude of backscattering. At lower beam energy, the depth from which the BSE are ejected tends to decrease and subsurface features become more difficult to detect.

A large proportion of BSE is emanated from close to the point where the beam is incident upon the specimen. The number of BSE ejected from locations farther away laterally decreases with increasing distance from this point. This pattern of lateral spatial distribution is generally true for both non-tilted and tilted specimens, varying only slightly. The BSE ejected from around the beam penetration area represent high-resolution signal, while the BSE emanating from remote lateral locations have undergone multiple elastic and inelastic scattering events and serve to degrade the image resolution. The farther is the ejection of the BSE signal from the beam impact point, the greater is its contribution to the noise in the image. High atomic number targets generate a large fraction of BSE close to the beam incidence point resulting in a high-resolution signal. Low atomic number targets generate a signal which has a large proportion of BSE ejected from remote locations, giving rise to low-resolution image.

3.4.1.10 Formation of Compositional or *Z* Contrast with BSE

It is clear from above that the contrast in an image formed by a backscattered detector is based on the differences in the mean atomic numbers of the elements in a sample. The heavy elements appear bright and the light elements appear dark in a backscattered image. Since the intensity of the BSE signal is related to the mean atomic number of the specimen, BSE images can provide information about the distribution of chemical phases in a specimen. Differences in the chemical composition of various phases in a localized region are exhibited in a BSE image. The Z contrast C_Z obtained from two locations will depend on the difference in their backscatter coefficient which varies directly with atomic number. If the BSE detector energy response is assumed to be the same for electrons derived from both locations, the C_Z between two regions can be expressed in terms of η as follows:

$$C_Z = \frac{\eta_2 - \eta_1}{\eta_2} \tag{3.17}$$

As shown in Fig. 3.21, two adjacent locations with the same chemical makeup (e.g., atomic number) will not exhibit any compositional contrast as they will exhibit the same backscatter coefficient. On the other hand, two locations with different Z will exhibit compositional contrast as they will yield different η, the value of which depends on their respective atomic number.

Backscattered detectors are usually annular in design placed directly above the specimen around the optic axis with a hole in the center to allow passage of electron beam. The detector is concentric with the electron beam. This design serves to maximize the solid angle of collection. BSE detectors are usually either of

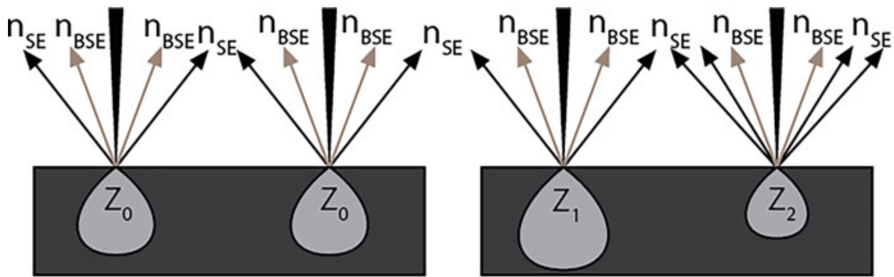

Fig. 3.21 (**a**) Number of SE and BSE produced from two adjacent flat locations of the same *Z* will be equal in number. *Z* contrast will not be visible. (**b**) Number of BSE produced from a location with high *Z* will be higher than those derived from low-*Z* location. Compositional or *Z* contrast will be seen with high-*Z* location appearing brighter than the low-*Z* location. The number of SE generated is taken to be the same from both adjacent locations. Adapted from [14]

solid-state semiconductor or scintillator-photomultiplier type. The solid-state device works when BSE derived from the specimen interact with Si to create electron-hole pairs (e.g., charge pulse) whose magnitude is proportional to the number and energy of the incoming BSE. The high number of pulses generates greater signal and corresponds to stronger contrast in the image. Scintillator type detector generates photons when BSE strikes its surface. The number of photons is proportional to the number of BSE interacting with the scintillator surface. Various contrast components can be selected by changing the geometry and position of the detector. Both detector types are not sensitive to low-energy electrons, thereby excluding detection of secondary electrons.

In *Z* contrast image, features with different densities will display different contrasts. However, features in a specimen with uniform density can also exhibit various levels of contrast depending on their orientation with respect to the location of the BSE detector. For instance, the features facing toward the detector will appear bright in the image. The features facing away from the detector will appear relatively dark even though they have the same density. This is due to the fact that BSE emitted from the specimen have straight trajectories and continue their travel in the direction they are originally emitted. A large proportion of BSE emitted from features facing the detector is more probable to enter the detector than the BSE ejected from features facing away from the detector. The signal thus produced by favorably oriented features whose surface is normal to the detector will be stronger. Apart from the atomic number *Z* component, this characteristic adds a directionality component to the BSE image. So the contrast in the BSE image depends not merely upon the average atomic number of the features (phases) in the specimen but also on the trajectory of the BSE emitted from those features. If the specimen is flat, the BSE trajectories will not vary and the contrast will solely depend on the *Z* component. If the surface is rough, the BSE trajectories will vary as per orientation of features and the image contrast will be composed of *Z* and trajectory components. Separation of

Z and trajectory components present in the BSE image can generate BSE compositional or topography images independently.

Separation of signals in the solid-state BSE detector is made by designing it in two segments A and B which are positioned on the opposite sides of the specimen surface (see Fig. 2.37). Each of these segments can receive signals and form an image independent of each other. Each segment is a semiconductor wafer that views the specimen from a different angle. Signals received by segments A and B can be added or subtracted to separate contrast in order to highlight specific features in the images. If the signals reaching both segments are added to get a sum BSE image (A + B), it will reveal compositional differences (*Z* contrast) present within the specimen (see Fig. 3.22a). To obtain this type of BSE COMPO image, both segments of the detector placed above the specimen are used to collect electrons symmetrically about the beam, and the resulting images are added. In this mode, the detector has a large collection angle and the electrons are collected from all azimuthal angles. Due to this collection method, the trajectory component of the contrast is eliminated since all trajectories are collected equally irrespective of the direction in which the electrons leave the specimen surface. Atomic number component of contrast dominates in this type of image where signal becomes stronger with increasing atomic number.

If the signals are subtracted (A − B), trajectory component of the signal is accentuated to highlight surface topography (see Fig. 3.22b). This type of image is known as BSE TOPO image. If the specimen is flat, backscattered signals recorded by opposite segments of BSE detector are similar. If the surface is rough, the strength of signal reaching the segments will vary depending on its orientation with respect to the surface topography. The features of the specimen that face a particular segment of the detector appear bright in the image formed by that segment (see Fig. 3.23). Subtraction of signal produces strong BSE topographic contrast that enhances surface features of the specimen. Atomic number contrast in this type of image is eliminated since *Z* components received by each segment are equal in magnitude and are canceled out.

In some SEMs, individual radial segments A and B of a BSE detector can be switched on or off to control the type of contrast produced. If a scintillator-photomultiplier detector is used, the difference in BSE trajectories can be exploited to enhance contrast by physically changing detector's position. Backscattered SEM images showing compositional and topographic views of thermal barrier coating and mineral samples obtained in the manner described above are shown in Fig. 3.24a, b and c, d, respectively.

In addition to the above, BEI SHADOW mode can be used by combining signals from two BSE detectors. The first detector is placed directly above the specimen and used in COMPO mode, and the second is displaced from the end of the objective pole piece and placed at an angle above the specimen. The second detector can be a retractable BSE detector whose position can be altered. The effect of combining the signals from two detectors is to introduce "shadowing" effects in the image which serves to enhance the 3-dimensional morphology and topography of the surface features. Shadow is produced in the image since BSE have relatively

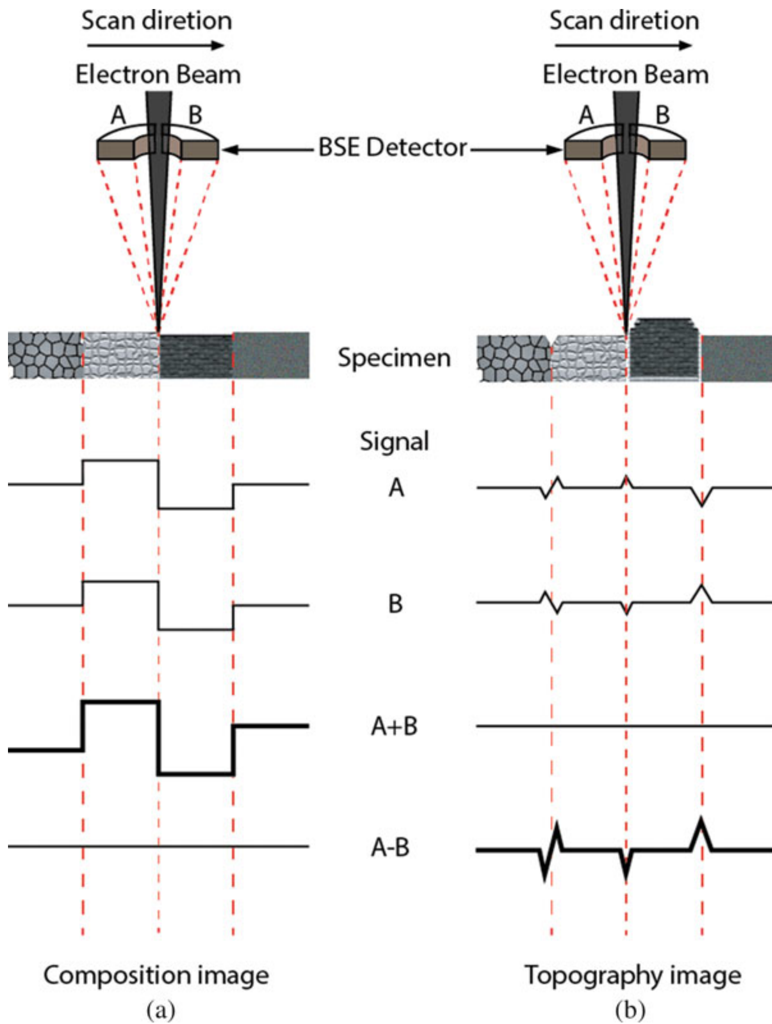

Fig. 3.22 The BSE image contains compositional and topographic information. The annular BSE detector located around the optic axis contains two segments A and B that receive signals independently of each other. (**a**) Addition of signals (A + B) gives compositional contrast, while (**b**) subtraction (A − B) gives topographic contrast [15]

straight trajectories and are blocked by the features in the specimen to reach the detector resulting in a shadow. At low magnification, BSE topographic contrast can be stronger than secondary electron topographic contrast due to sharp shadow effects obtained with a BSE detector positioned at a narrow angle relative to the specimen surface.

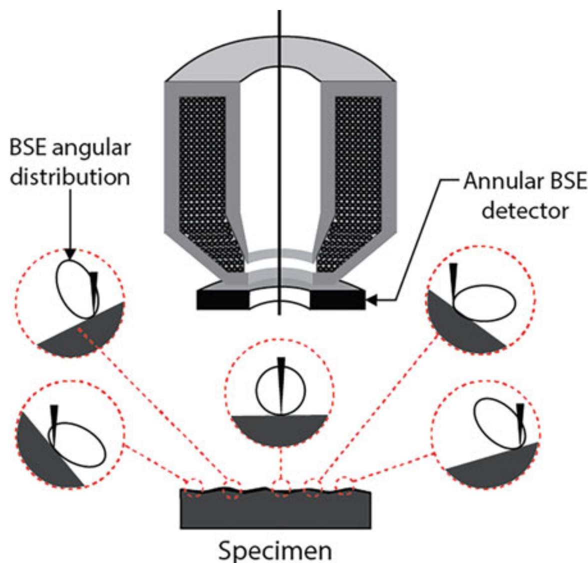

Fig. 3.23 Schematic showing angular distribution of BSE from a rough specimen surface. The features of the specimen that face a particular segment of the BSE detector will appear bright in the image formed by that segment. The same feature will appear dark in the image formed by the other segment

3.4.1.11 Spatial Resolution of BSE Images

The spatial resolution of backscattered electron images varies between 50–100 nm for beam energies of 10–20 keV that are employed during routine imaging. The resolution is several orders of magnitude worse than that obtained in secondary electron images. This is directly related to the comparably large volume within the specimen from where the backscattered electrons are derived to form the image. Still, BSE imaging allows distinguishing between chemically distinct phases at a far better resolution than that offered by x-ray microanalysis. New technological advances such as low beam energy combined with small spot size produced by modern field emission guns can be used to reduce the BSE source volume within the specimen to a few nanometers taking it closer to the spatial resolution achieved by secondary electrons. At low beam energy of 1 keV, the information volume of SE and BSE become comparable. For high-resolution microscopy, low-loss BSE are used which are ejected from the area immediately surrounding the point of beam incidence. These electrons undergo single or lesser number of scattering events and represent high-resolution signal.

3.4.1.12 Applications of Backscattered Electron Imaging

Backscattered electron imaging is a valuable imaging tool and provides a quick qualitative method to locate phases with different chemical compositions which then can be further investigated using elemental chemical analysis. Backscattered images reveal the distribution of phases/compounds with different compositions based on the differences in their mean atomic numbers (see Fig. 3.25a). It is particularly useful for the study of multiphase materials, catalysts, segregation at grain boundaries, and

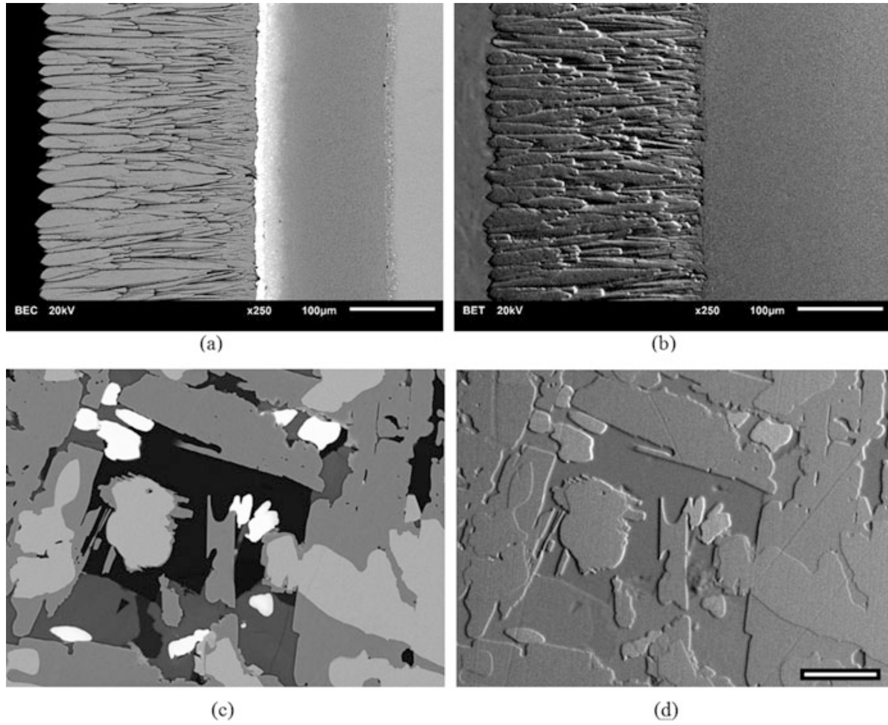

Fig. 3.24 Backscattered electron images obtained from a specimen of thermal barrier coating showing (**a**) BSE compositional contrast, COMPO mode (A + B), and (**b**) BSE topographic contrast, TOPO mode (A – B). Similarly, backscattered (**c**) compositional and (**d**) topography images obtained from a mineral sample showing multiple phases. Signals reaching both sectors of BSE detector are added to get a sum image, revealing compositional differences present within the specimen (see **a** and **c**). Signals are subtracted to highlight surface topography (see **b** and **d**)

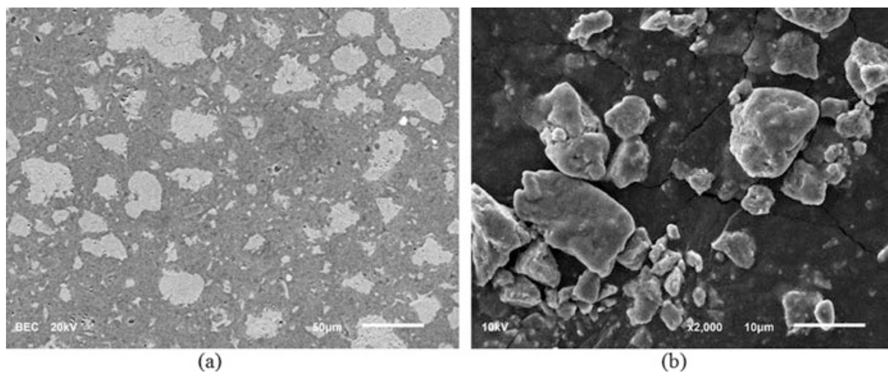

Fig. 3.25 BSE images of (**a**) polished cement sample showing differences in the magnitude of contrast formed between different phases depending on their mean *Z*, (**b**) catalyst specimen

contaminants (see Fig. 3.25b). Heavy metal oxides, nitrides, or carbides appear bright in a relatively low-Z matrix such as steel. Similarly, grain or domain boundaries can be observed distinctively in a BSE image without having to etch the specimen. Likewise, BSE imaging can reveal the presence of subsurface cracks, voids, or defects. BSE imaging is especially useful in observing biological specimens. Since the BSE yield of biological specimens is low, heavy elements such as lead, silver, or gold are attached to active molecular groups present in the specimen in a process called *staining*. These locations appear bright and the rest of the material appears dark in the BSE images. These locations are identified conveniently when compared to secondary electron images.

BSE imaging can be used to extract compositional information from nanoscale materials in the modern SEM equipped with field emission gun. At low beam energy, the volume of the specimen from which the BSE is derived approaches that of high-resolution SE_1 signal. This characteristic can be exploited to study the morphology and spatial distribution of nano-features in various nanoscale materials. Delicate specimens can be observed as electron beam-induced damage is reduced. Similarly, nonconducting or insulator materials can be examined with high spatial image resolution.

3.4.1.13 Limitations of Backscattered Electron Imaging

Contrast produced by BSE imaging depends largely on the difference in the average atomic number of various phases present within a multiphase specimen under observation. It is possible to produce two different phases with the same mean Z but having very different chemistry by mixing several elements in various proportions. The BSE images obtained from such material will not show appreciable contrast that can distinguish one phase from the other even though their chemical makeup is dissimilar [16]. Likewise, backscattering increases monotonically with atomic number, but deviation from this generally observed behavior has been reported in the literature [17]. Also, the backscattering coefficient can be influenced by the magnetic domains of a material [18]. In such cases, BSE image will fail to produce contrast that corresponds to the mean Z of the material examined. Although valid, these limitations are only encountered under exceptional circumstances and do not diminish the benefits of BSE imaging. The Z contrast formed between two phases with a comparable mean atomic number is quite weak as discussed in Sect. 3.4.1.4. This necessitates the use of well-polished flat specimens to increase the BSE collection efficiency of the detector. Likewise, short working distance and use of large detector surface area help to maintain an adequate signal-to-noise ratio.

3.4.2 Topographic Contrast (Secondary Electron Imaging)

3.4.2.1 Secondary Electron Yield

The extent of secondary electron generation in a specimen is expressed in the form of secondary electron coefficient (δ) which is defined as the ratio of the number of

secondary electrons emitted from a specimen to the number of incident beam electrons that enter the specimen, as shown below:

$$\delta = \frac{n_{SE}}{n_B} \tag{3.18}$$

where

δ = total secondary electron coefficient

n_{SE} = number of secondary electrons

n_B = number of incident beam electrons

Secondary electron coefficient can be measured in terms of the ratio of secondary electron current emitted out of the specimen to that of the incident beam current.

$$\delta = \frac{i_{SE}}{i_B} \tag{3.19}$$

where

δ = secondary electron coefficient

i_{SE} = secondary electron current moving out of the specimen

i_B = electron beam current entering the specimen

3.4.2.2 Escape Depth of SE

Secondary electrons have low kinetic energy which enables them to leave the surface from shallow depth only. SE generated within a few nanometers of specimen surface can eject out of the specimen. SE generated away from the surface cannot escape the specimen as they lack enough energy to propagate through the solid to reach the surface and are therefore lost within the specimen. This effectively sets the escape depth for SE to a few nanometers. Therefore, the entire population of secondary electrons, generated by incident electrons at depths beyond the escape range, is not utilized for imaging.

All the random electron trajectories within the specimen are associated with the production of secondary electrons. Generation of SE relies on inelastic scattering; therefore as they pass through a specimen, their energy continually decrease. If the SE happen to reach the specimen surface, they still need enough kinetic energy (several electron volts) to overcome the potential surface barrier (work function) of the specimen. The produced secondary electrons are heavily attenuated due to inelastic scattering when they try to escape the specimen surface. The probability of the SE to leave the specimen surface is given by:

$$p(z) = 0.5 \exp\left(-\frac{z}{\lambda}\right) \tag{3.20}$$

where p is the probability, z is the depth below the surface where the SE is produced, and λ is the mean free path or the escape depth of the SE. It can be seen from Eq. 3.20 that the probability of escape of SE decreases exponentially as the depth at which they are generated increases. The maximum depth of emission is 5 times the escape depth of the SE (i.e., 5λ) [19]. The escape depth depends on the type of material. It is

smaller (around 1 nm) in metals and up to 20 nm in insulators. This is due to the fact that SE generated within the specimen are inelastically scattered due to the presence of a large number of conduction electrons in metals. This scattering prevents the SE generated within greater depths of metals to escape the surface. Due to a lack of electrons in insulators, inelastic scattering of generated SE is not significant, thus allowing them to reach and escape the specimen surface from greater depths. Values quoted above are a rough estimate. In actual practice, the energy of SE will determine the mean free path so that SE with 0–50 eV range will correspond to a range of λ.

The probability of escape of secondary electrons as a function of specimen depth Z is shown in Fig. 3.26 which shows a sharp decrease in the escape probability with depth. In the range of 10–30 keV, secondary electron escape depth is around 100x smaller than the backscattered electron escape depth.

3.4.2.3 Energy Distribution of SE

The energy distribution of the electrons ejected from a specimen is spread over all energy range, i.e., from zero to the energy of the incident beam E_0. When the high-energy electron beam penetrates the specimen, it can knock out weakly bound outer shell electrons of atoms of metals, semiconductors, and insulators. There is a significant difference between the energy of the beam (keV) and that of the electrons belonging to a specimen (eV) in a collision event. Due to this reason, only a small portion of the beam kinetic energy is likely to be transferred to the specimen atom resulting in the ejection of low-energy electrons. High-energy electrons can also be ejected during the interaction of the beam with tightly bound electrons of the atom. However, the probability of ejection of such electrons is low. These electrons do not

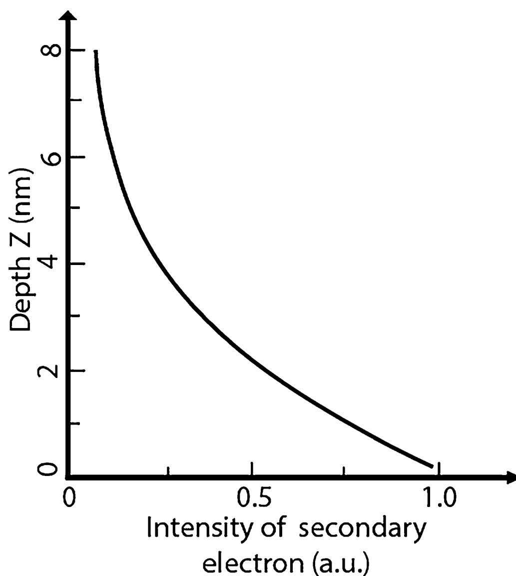

Fig. 3.26 With an increase in the depth of SE generation, the probability of SE escaping to the surface decreases [20]

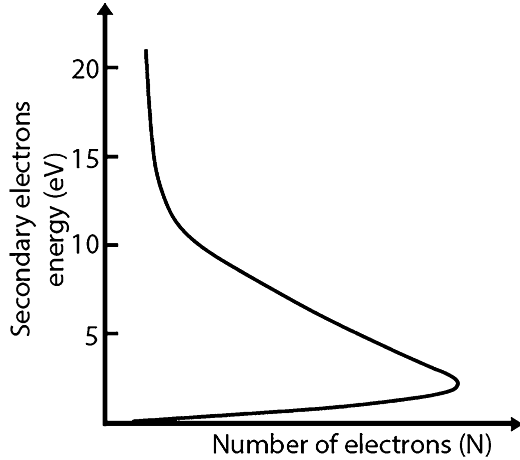

Fig. 3.27 Plot showing energy distribution of secondary electrons. Majority of the SE generated have a kinetic energy of 2–5 eV [20]

contribute significantly to the formation of secondary electron images due to their low numbers.

The secondary electrons that escape the specimen surface usually have a very low kinetic energy, i.e., below 50 eV. The distribution of the secondary electron energy is generally peaked in the range (2–5 eV) as demonstrated in Fig. 3.27. Although the secondary electron energy can be up to 50 eV, 90% of secondary electrons have an energy <10 eV. A small number of low-energy backscattered electrons are included in secondary electron energy range and are thus counted as secondary electrons. But the effect of this quantity is negligible.

3.4.2.4 Types of SE Signal (SE_1, SE_2, SE_3, SE_4)

The secondary electron signal obtained from a specimen is composed of two types of secondary electrons designated as SE_1 and SE_2 [21]. The secondary electrons that are produced within the narrow escape depth of the specimen (i.e., within 5λ) by the incident electron beam impinging upon the specimen surface are called SE_1 (see Fig. 3.28). These electrons make up the high-resolution image that encompasses lateral spatial resolution as well as shallow sampling depth of the signal. Not all secondary electrons are produced by primary beam incident on the specimen surface. Secondary electrons are also produced in an indirect manner by the backscattered electrons that are generated within the specimen through elastic scattering and are emerging out of the specimen. These backscattered electrons inelastically scatter secondary electrons which in turn can emanate from the surface if present within the escape depth of the specimen. These secondary electrons are known as SE_2 (see Fig. 3.28). SE_1 and SE_2 are spatially separated as long as appreciable beam energy is employed. SE_1 originates close to the beam impact point while SE_2 is generated away from the probe from a region comparable to electron range of primary beam.

SE_2 is a low-resolution signal that carries different information than SE_1. SE_2 possess lateral and depth characteristics of the BSE signal that generates such signal.

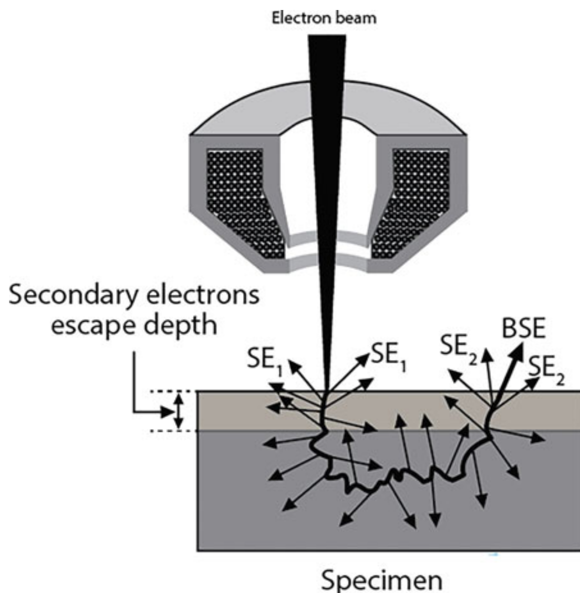

Fig. 3.28 SE_1 is generated close to the beam impact point and represents a high-resolution signal. SE_2 originates from an area away from the beam and represents a low-resolution signal

Change in SE_2 signal depends on the change in the backscattered signal. This could be understood by considering the fact that the extent of backscattering in a specimen with low Z is lower and it is higher in a specimen with high Z. High backscatter coefficient η in high-Z material will result in the production of the stronger SE_2 signal. This increase in SE_2 signal will produce a stronger contrast and the corresponding region will appear brighter in the image. This contrast is dependent on Z of the material and represents BSE imaging contrast rather than SE topographic contrast because the generation of SE does not change appreciably with a change in Z. Therefore, SE_2 signal is considered to signify BSE contrast.

The backscattered electrons propagate through the solid and reach the surface at much smaller angles compared to the primary beam that enters the surface at right angles. This results in greater electron path length increasing the chance of inelastic scattering of secondary electrons near the specimen surface giving rise to the stronger SE_2 signal. Additionally, backscattered electrons have lower energy compared to the primary beam and thus generate secondary electrons more efficiently. Due to this reason, the strength of the SE_2 signal is much higher than SE_1; however current density distribution of SE_1 is greater. At high magnifications (i.e., small pixel size), the resolution of SE image is thereby determined by the SE_1 signal while SE_2 serves to contribute to the background. The signal-to-noise ratio in high-resolution images is low due to the low strength of the SE_1 signal. At mid-range magnifications, the pixel size increases (compared to that at high magnification) and approaches the range of SE_2 signal which now determines the image resolution and contrast as it constitutes the predominant part of the detected signal.

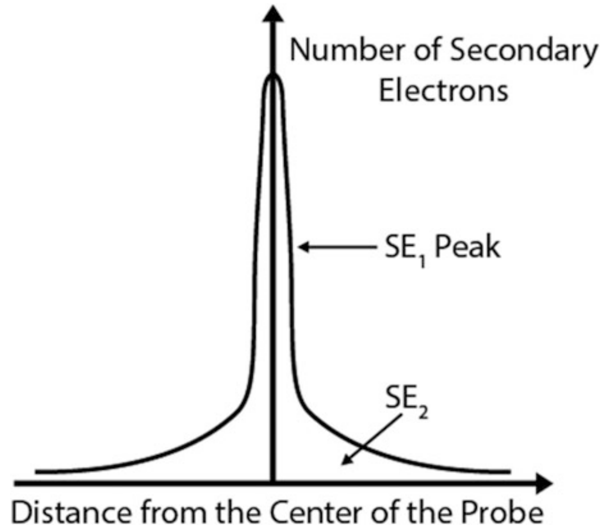

Fig. 3.29 Schematic representation of the variation in the intensity of the SE signal as a function of distance from the center of the probe, i.e., spatial distribution of SE_1 and SE_2 signal. SE_1 signal is generated by the incident probe while SE_2 is produced indirectly by elastically scattered BSE away from the beam incident point. The strength of the SE_2 signal is usually higher than SE_1; however since SE_2 is generated from a much larger area, the current density distribution of SE_1 is greater

Figure 3.29 shows the intensity of the SE signal as a function of distance from the incident probe. The central peak (SE_1 signal) is generated by the incident beam electrons and thus resembles the intensity distribution profile of the probe itself [22]. The FWHM of this peak and incident probe is similar. SE_2 signal is generated farther away from the probe by beam electrons undergoing multiple scattering events. The intensity of the SE_2 signal is low but it is spread out over a greater area.

The contribution of the SE_1 signal in secondary electron emission is greater than SE_2 signal in light elements. This is due to the fact that backscattering is low in light elements due to their small atomic size. Therefore, the main component of the total SE signal is generated by the primary beam incident on the specimen surface. In heavy elements, SE_2 signal dominates since backscattering is prominent due to large atomic size.

High-energy backscattered electrons ejected from the specimen with favorable trajectories are incident upon the metallic parts of the SEM such as chamber walls, objective lens, final aperture, etc. These BSE interact with various parts of the SEM chamber to generate indirect secondary electrons which eventually find their way into the detector and form part of the SE image (see Fig. 2.32). These secondary electrons are termed SE_3 and SE_4 signal. SE_3 are generated from the walls of the specimen chamber. SE_4 signal originates from the final aperture. SE_3 and SE_4 contribute to the SE signal but will depend on the extent of backscattering in the specimen and hence represent BSE imaging contrast. These signals are low-resolution signals that will contribute to the noise in the image.

3.4.2.5 Effect of Beam Energy on SE Yield

Secondary electron emission is higher at lower incident beam energy. There is a significant increase in secondary electron emission below 5 keV. This is due to the

Table 3.2 Secondary electron emission coefficient (δ) as a function of beam energy [23]

Element	5 keV	20 keV	50 keV
Al	0.4	0.14	0.05
Au	0.7	0.2	0.1

fact that secondary electrons have low energy and can only escape the specimen if they are generated near its surface. At low keV, the penetration of incident beam is shallow and most of the secondary electrons are generated near the specimen surface. This enables them to escape resulting in a higher secondary electron coefficient (δ) at lower beam energy. Table 3.2 demonstrates experimental values for the secondary electron coefficients for Au and Al over a range of beam energies [23].

Schematic representation of the total emitted current as a function of beam energy is shown in Fig. 3.30a. As the beam energy is decreased from a higher to a lower value, total electron coefficient denoted by ($\eta + \delta$) increases to a value of unity (upper crossover energy E_2 in Fig. 3.30a). Further decrease in beam energy will result in values higher than 1 which implies that the number of electrons emitted out of the specimen due to backscattering and secondary electron emission surpasses those supplied by the beam. Increase in the production of total electron coefficient within the escape depth of the electron beam results primarily due to an increase in secondary electron coefficient δ at low electron beam energy. Further reduction in the beam energy produces a peak in total electron coefficient followed by a decrease back to unity (lower crossover energy E_1 in Fig. 3.30a) and below. At beam energy range between E_1 and E_2, the specimen will not charge as the total electron yield exceeds the beam current entering the specimen. For values of incident energy above E_2, the total yield becomes less than 1 because the beam penetrates too deep into the specimen restricting ejection of BSE and SE, resulting in charge buildup. For values of incident energy below E_1, the total yield becomes less than 1 because the primary beam lacks enough energy to create SE again resulting in negative charging.

The upper crossover energy E_2 represents a suitable beam energy point for imaging. It is in the range 0.5–2 keV for organic materials and 2–4 keV for inorganics. Insulators can produce very high total electron coefficients at low beam energies. Values of E_2 have been tabulated for various materials in Table 3.3.

At low beam energy, the SE_2 electrons are generated closer to the beam impact point decreasing the range of SE_2 signal. SE_2 spatial distribution approaches that of SE_1 under such conditions. At low beam energy, SE_1 and SE_2 signals cannot be spatially separated even at high magnifications (i.e., with small pixel size). Due to their close proximity to the beam impact point, both types of signals now serve to make up the high-resolution image. Use of low beam energy, therefore, allows exerting better control on interaction volume and image contrast and facilitates the acquisition of high-resolution images rich in near-surface information (see Fig. 3.30b, c). The probe size, however, will be coarser at low beam energies. Aberration correction is used to overcome deleterious effects of low beam energy.

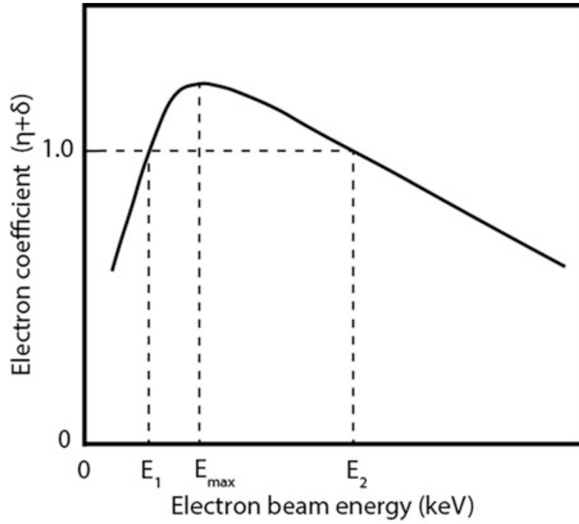

(a)

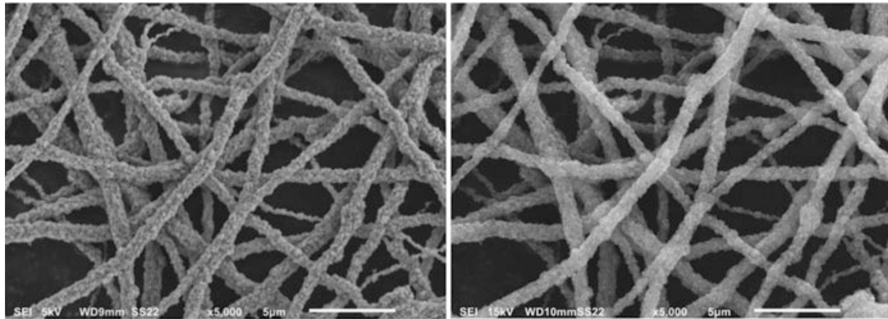

(b) (c)

Fig. 3.30 (**a**) Plot illustrating the change of total emitted electron coefficient ($\eta + \delta$) with beam energy. Upper crossover energy point E_2 represents optimal beam energy to image materials. It is in the range 0.5–2 keV for organic and 2–4 keV for inorganic materials. (**b**) SEM image at low beam energy showing surface features. (**c**) Same sample: some features are lost at high beam energy

Table 3.3 Upper crossover energy E_2 for various materials

Material	E_2 (keV)	Reference
Electron resist	0.55–0.70	[24]
5% PB7/nylon	1.40	[24]
Acetal	1.65	[25]
Polyvinyl chloride	1.65	[25]
Teflon	1.82	[25]
Glass passivation	2.0	[24]
GaAs	2.6	[24]
Quartz	3.0	[24]

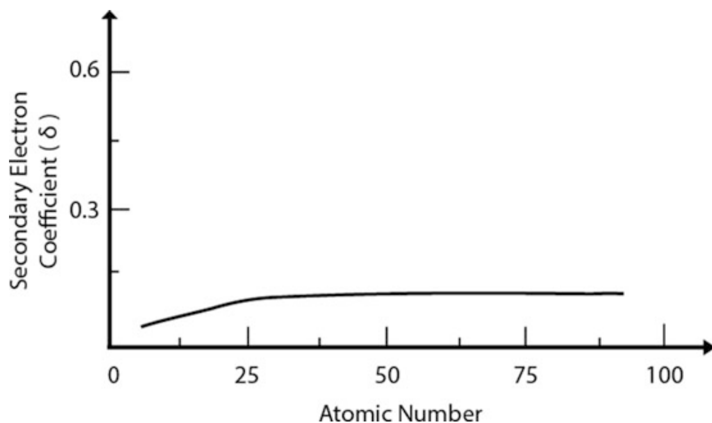

Fig. 3.31 Secondary electron coefficient does not change appreciably with increasing atomic number

3.4.2.6 Effect of Atomic Number on SE Yield

For practical considerations, the secondary electron emission can be considered to be independent of the atomic number and does not change significantly from light to heavy elements, as shown in Fig. 3.31 [26]. For an electron beam energy of 20 keV, the value of the secondary electron yield δ for most elements is approximately 0.1 [26]. However, gold and carbon are not constrained by this value. Gold has a significantly high value of secondary electron yield of 0.2, whereas carbon has a low yield value of around 0.05. The secondary electron emission is greatly dependent on the surface condition of the specimen. Contamination at the specimen surface can pose a significant hindrance to the ejection of low-energy SE from within the target material.

3.4.2.7 Effect of Tilt on SE Yield

When the specimen is tilted at increasing angles θ, secondary electron coefficient δ increases obeying a mathematical relation that can be approximated as follows [27]:

$$\delta(\theta) = \delta_0 \sec \theta \tag{3.21}$$

where δ_0 represents the δ value at zero tilt (i.e., when the beam is perpendicular to the specimen surface). This relationship is expressed using the schematic shown in Fig. 3.32a, b. At 45° tilt, the primary electron beam path length d increases to $d = d_0 \sec \theta$, while the escape depth of SE, d_0, remains the same. Increased path length within the escape depth results in the generation of a larger number of SE that are ejected giving rise to increased δ. Moreover, since the degree of backscattering increases with tilt, SE generated due to backscattering also increase. When beam energy is reduced to the level of E_2, all of the SE generated can escape even at zero tilt. So, tilting a specimen at low beam energy does not serve to increase δ any further.

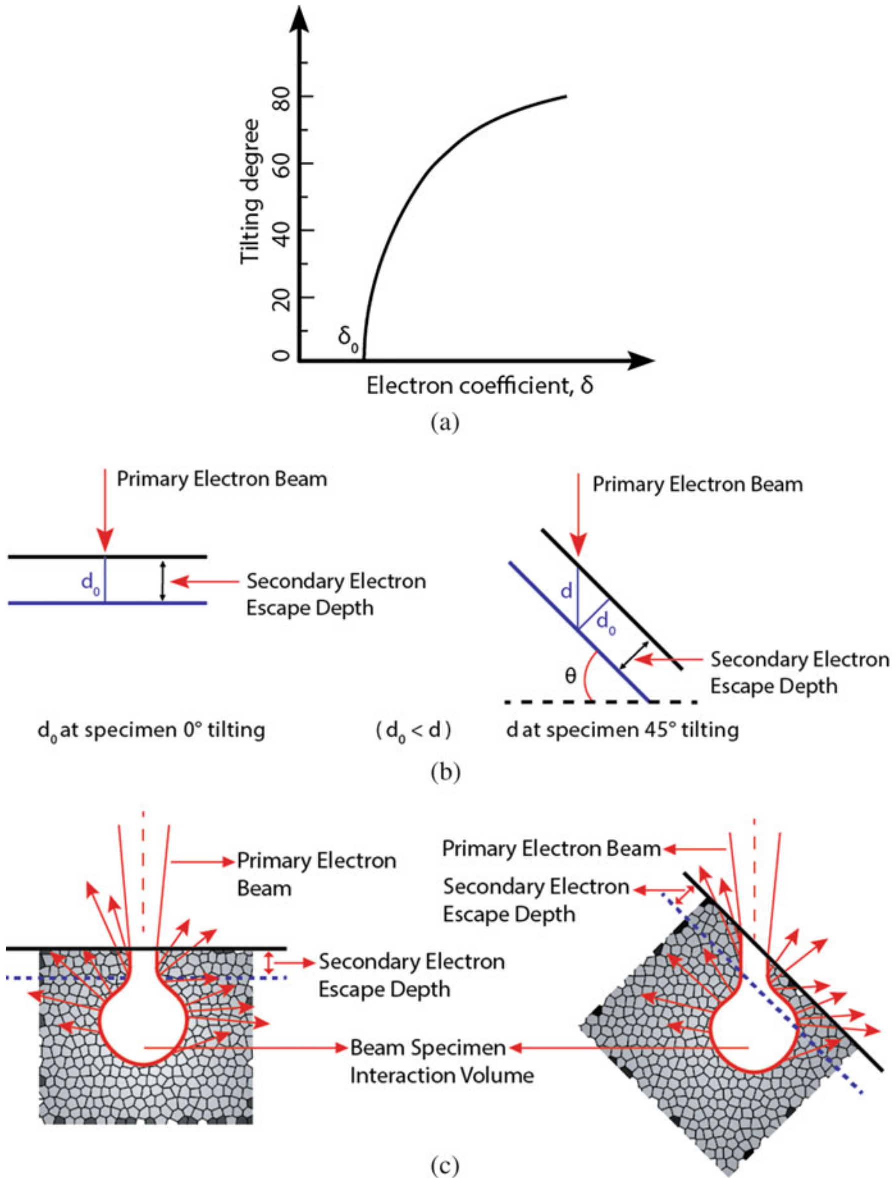

Fig. 3.32 (**a**) Plot showing increase in δ with tilt follows a secant relationship. (**b**) Specimen tilt increases the beam path length within a distance of escape depth. This results in the production and escape of a larger number of SE. (**c**) A large part of the interaction volume becomes close to the specimen surface when it is tilted making it more probable for the SE to escape

As shown in Fig. 3.32c, high angle of tilt increases the length of the primary electron path within a distance of escape depth, while keeping the specimen surface closer to the propagating electron beam. Once the primary beam loses sufficient energy to generate inelastically scattered secondary electrons, a significant proportion of it is still within the narrow escape depth of the tilted specimen. This results in an increased secondary yield.

3.4.2.8 Directional Dependence of SE Yield

The emission of secondary electrons is governed by a cosine function of ϕ which is an angle measured from the surface normal. The SE yield remains unaffected by tilt. This is due to the fact that SE are produced isotropically by the incident electrons independent of tilt. Even though the total SE coefficient δ increases with the degree of tilt, the angular distribution of emission does not change. This is because the distribution of path lengths obeys a $1/\cos\phi$ distribution relation relative to the surface normal irrespective of the tilt.

3.4.2.9 Formation of Topographic Contrast with SE

The SEM is most frequently used to examine the shape, size, and surface texture of features in a specimen providing information about the latter's topography and morphology. Secondary electrons (SE) are considered to constitute the most appropriate signal to study the surface topography of specimens. This is due to the fact that the energy of secondary electrons is low and these electrons are only emitted from the topmost layers of the specimen. This enables examination of surface features only without contribution from signals from greater depths of the specimen resulting in observation of surface topography. Mode of imaging undertaken using secondary electrons is generally known as secondary electron imaging (SEI). This is the most common type of imaging used in the SEM. As an example, the secondary electron image of the charcoal sample is shown in Fig. 3.33.

E-T Detector

In the SEI mode, the signal results from the interaction of the electron beam with atoms at or near the surface of the specimen. The interaction of the incident beam with specimen results in inelastic scattering events, and low-energy ($\approx$50 eV) secondary electrons are ejected from the loosely bound outermost shells of specimen atoms. Due to their low energy, electrons located within a few nanometers of the sample surface are able to escape and are used to generate topographic contrast. After their ejection from the specimen surface, the electrons are collected using the Everhart-Thornley (E-T) detector which is scintillator-photomultiplier system placed inside the SEM chamber at an angle to the specimen surface. The strength of the signal depends on the number of SE reaching the detector. This is why surface features facing toward the direction of the E-T detector generate higher contrast compared to those facing away from it. Low-energy secondary electrons are pulled toward the detector under a positive bias (+200–300 V) in the form of a wire mesh/grid/collector (Faraday cage) placed at the front end of the detector. The electrons pass through the grid and strike the scintillator surface of the detector. The secondary

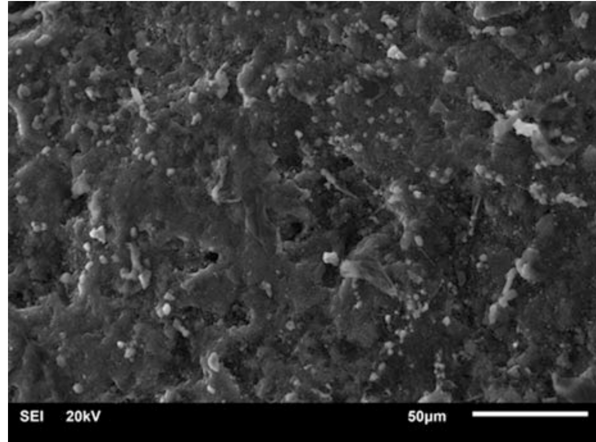

Fig. 3.33 Secondary electron image of charcoal dipped in colloidal Au showing surface topography

electrons reaching the detector possess the energy of only a few electron volts (eV) which is not adequate to generate a viable signal from the scintillator. The scintillator surface made of a plastic or crystalline material is therefore covered by a thin metal coating that is under a + 10 kV positive bias which serves to accelerate the incoming electrons onto scintillator. The electrons are converted into light (e.g., cathodoluminescence) upon striking the scintillator surface. The light then passes through a transparent pipe to reach a photomultiplier tube which converts the light into an electric signal that is amplified to levels suitable for the formation of an image. It is then converted into a digital signal and displayed on a monitor as a two-dimensional intensity distribution map. E-T detector is commonly referred to as the SE detector as the images produced are dominated by SE contrast when the collector is positively biased. Working principle of E-T detector is discussed in detail in Sect. 2.6.1.

Factors Affecting Topographic Contrast

The three-dimensional appearance of SEM images is due to differences in contrast between various structural features of the specimen when they are displayed on the viewing monitor. Contrast arises when different parts of the specimen generate varying amounts of secondary electrons when the electron beam strikes them. Areas which generate large numbers of secondary electrons will appear brighter than areas that generate fewer secondary electrons. The yield of secondary electrons by various areas may be influenced by several conditions. The orientation of the specimen topography relative to the electron beam and secondary electron detector greatly affects the yield of secondary electrons. Tilted features in a specimen yield more SE as secondary electron coefficient δ increases as a secant function of tilt θ. Yield of SE from tilted surfaces is not significantly different in various directions, so the trajectory component in the SE signal is negligible. Backscattered electrons also find their way into the E-T detector to contribute to the SE image. The Everhart-Thornley detector will receive line-of-sight BSE from features of specimen facing

the detector. These BSE will form part of the SE image. In addition, tilted surfaces in a specimen will generate a higher number of BSE as backscatter coefficient η increases significantly with the angle of tilt. This will, in turn, increase the SE_2 signal. Moreover, titled features will generate BSE in a direction defined by the beam direction and surface normal of the feature. This adds a trajectory component to the SE image. Elements with high atomic number elements have a higher yield of backscattered electrons compared to elements with lower Z. This adds a number component to the topographic contrast, and high-Z elements therefore, may appear brighter in the SE image. High accelerating voltage results in lower contrast due to greater beam penetration and enhanced secondary yield from all parts of the specimen topography. Contrast can be enhanced by using lower accelerating voltage. Charge accumulation or buildup in partly coated areas of the specimen can also result in an increase in contrast. Uncoated areas tend to build up a static charge from the electron beam and cannot dissipate the charge rapidly enough. This may cause the deflection of the beam so that it strikes other areas to generate an excessive number of secondary electrons that form part of the image contrast. Likewise, naturally magnetic areas in a specimen may either deflect or attract the beam to affect the yield of SE. When crystals are oriented along certain lattice planes relative to the beam, an enhanced yield of SE may result in an increase in brightness along these lattice planes so that certain crystals will appear much brighter than others. In short, there is a large number of factors that influence the formation of contrast in SE image.

Edge Effect

Secondary electrons are emitted from all features that interact with the incident electron beam. However, the strength of the signal obtained due to secondary electrons depends greatly on the orientation of surface features of the specimen with respect to the incident beam. Greater variation in the orientation of features (i.e., higher surface roughness) results in greater variation in secondary electron signal from one location of the specimen to the other giving rise to higher topographic contrast. The number of secondary electrons emitted from specimen surface changes with the angle of incidence of the electron probe on that surface. If the incident beam is perpendicular to the surface, the interaction volume within the specimen is uniform about the beam axis resulting in the generation of a certain number of electrons. Higher incidence angle allows greater penetration of the beam into surface regions such that the escape distance toward one side of the beam decreases, and the number of secondary electrons emitted from the specimen increases. Higher secondary electron emission results in a brighter contrast. This is why thin raised areas, steep surfaces, protrusions, and edges within a specimen where interaction volume intercepts these regions tend to appear brighter compared to the broad flat surfaces. This phenomenon is called *edge effect* since it takes place along sharp edges in a specimen. These areas appear brighter because the secondary electrons are able to escape from all sides of the thin areas. Schematic in Fig. 3.34 shows this effect for various edge shapes.

The higher the accelerating voltage used during imaging, the greater the edge effect. This phenomenon is more pronounced when an uneven surface such as coil

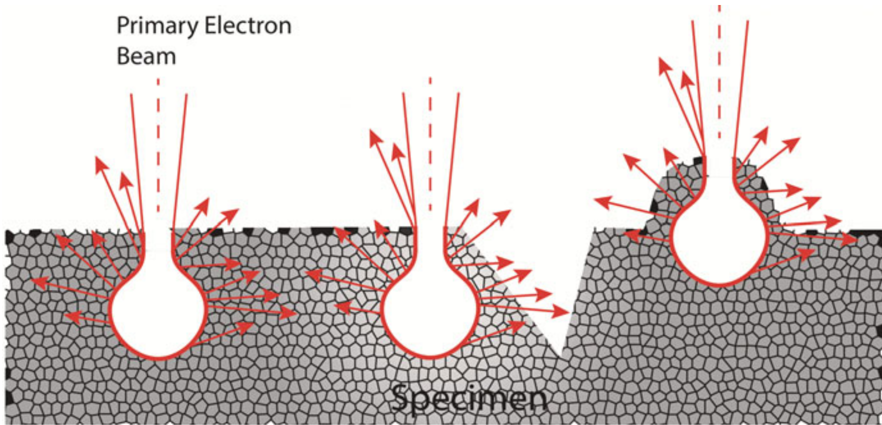

Fig. 3.34 Schematic showing the phenomenon of the edge effect. Edges, steps, and protrusions in a specimen appear bright due to generation and escape of a larger number of secondary electrons from these regions

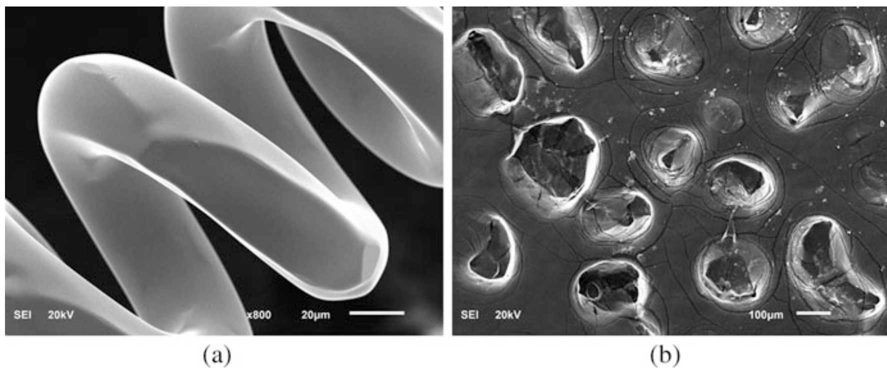

Fig. 3.35 Secondary electron image showing bright edges of (**a**) coil and (**b**) holes in carbon tab samples, due to the emission of a large number of SE

sample is examined in the SEM. The edges of the coil and holes in carbon tab samples appear brighter than the rest of the material as shown in Fig. 3.35a, b, respectively.

Spherical Particles

As mentioned earlier, the yield of secondary electrons is also affected by the angle that the beam enters the specimen surface. If the beam enters a specimen at a 90° angle, the beam penetrates directly into the specimen, and any SE generated below a certain depth will not be able to escape. On the other hand, if the beam strikes the specimen in a grazing manner, then the beam does not penetrate to a great depth (along the surface normal), and more SE will be able to escape since they are closer

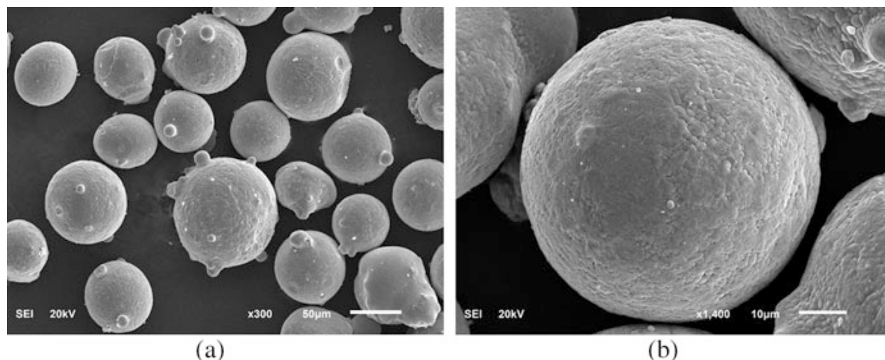

Fig. 3.36 (**a**, **b**) Secondary electron SEM images showing strong contrast at the edges of round particles of NiCrAlY powder specimen

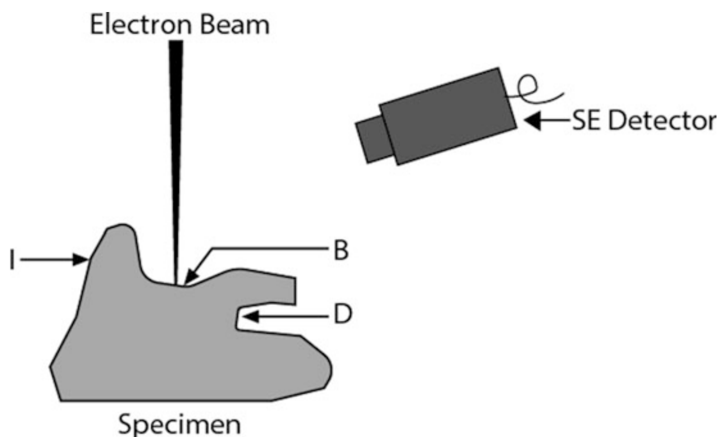

Fig. 3.37 Schematic diagram showing the effect of the irregular-shaped specimen on the SE image contrast [28]

to the surface. Since rounded objects are more likely to be grazed by the electron beam than would flat objects, round areas usually appear to have a bright line around them due to the enhanced yield of SE (see Fig. 3.36a, b).

Non-regular Specimens

As illustrated in Fig. 3.37, certain areas of the specimen (designated "D") will not be struck by the beam and will not yield any secondary electrons. These areas will appear dark in the image. Areas such as "I" in Fig. 3.37 will be struck by the beam, but since they face away from the detector, fewer secondary electrons will be collected and intermediate levels of brightness will be displayed in the image. Optimal yields of secondary electrons would come from areas that are struck by

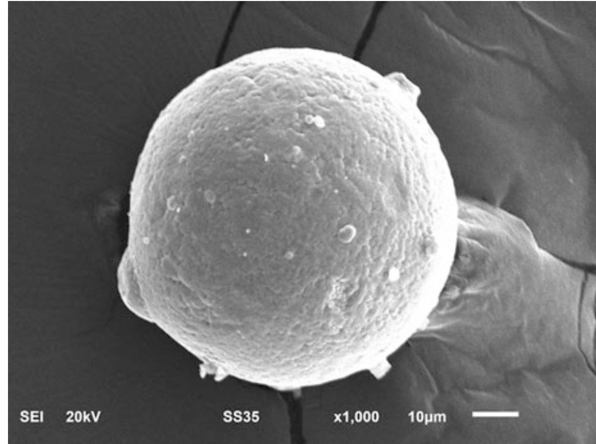

Fig. 3.38 Secondary electron SEM image of NiCrAlY powder particle placed over a C tab. E-T detector is located toward the right-hand side of the specimen. It can be seen that the surface facing the E-T detector appears bright. The C tab appears dark indicating organic material

the beam and face the detector ("B" in Fig. 3.37). These areas would appear as highlights in the image.

Effect of Lateral Placement of E-T Detector

The contrast in the SE image partly depends on the direction where the E-T detector is placed as shown in Fig. 3.38. The features of the specimen facing the detector will appear brighter as the collection of SE from that region will be the maximum. Features facing away from the detector shall appear less bright. Organic materials will appear dark due to low SE yield.

References

1. Newbury DE, Myklebust RL (1979) Monte Carlo electron trajectory simulation of beam spreading in thin foil targets. Ultramicroscopy 2(9):391–395
2. Sim SK, Teh V (2015) Image signal-to-noise ratio estimation using adaptive slope nearest-neighbourhood model. J Microsc 260:352–362. https://doi.org/10.1111/jmi.12302
3. Frank J, Al-Ali L (1975) Signal-to-noise ratio of electron micrographs obtained by cross correlation. Nature 256:376–379. https://doi.org/10.1038/256376a0
4. Erasmus J (1982) Reduction of noise in TV rate electron microscope images by digital filtering. J Microsc 127:29–37
5. Yeap ZX, Sim KS, Tso CP (2016) Signal-to-noise ratio estimation technique for SEM Image using linear regression, Proc. of 2016 international conference on robotics, automation and sciences (ICORAS) 5–6 Nov. 2016. https://ieeexplore.ieee.org/stamp/stamp.jsp?tp=&arnumber=7872602. Date accessed 19 Sept 2018
6. Thong JT, Sim KS, Phang JC (2001) Single-image signal-to-noise ratio estimation. Scanning 23:328–336. https://doi.org/10.1002/sca.4950230506
7. Sim KS, Thong JTL, Phang JCH (2006) Effect of shot noise and secondary emission noise in scanning electron microscope images. Scanning 26:36–40. https://doi.org/10.1002/sca.4950260106
8. Henoc J, Maurice F (1991) In: Heinrich KFJ, Newbury DE (eds) Electron probe quantification. Plenum Press, New York, p 105

9. Hovington P, Drouin D, Gauvin R (1997) CASINO: A new Monte Carlo code in C language for electron beam interaction - Part I: Description of the program. Scanning 19(1):1–14
10. Kanaya K, Okayama S (1972) Penetration and energy-loss theory of electrons in solid targets. J Phys D 5:43
11. Reimer L (1998) Scanning electron microscopy: physics of image formation and microanalysis, 2nd edn. Springer, Heidelberg
12. Reuter W (1972) In Proc. 6th international congress on X-ray optics and microanalysis, Shinoda G, Kohra K, and Ichinokawa T (ed), University of Tokyo Press, Tokyo, p. 121
13. Heinrich KFJ (1966) In Proc. 4th international conference on X-ray optics and microanalysis, Castaing R, Deschamps P, and Philibert J (eds.), Hermann, Paris, p. 159
14. Goldstein JI, Newbury DE, Joy DC, Lyman C, Echlin P, Lifshin E, Sawyer L, Micheal JR (2003) Scanning electron microscopy and X-Ray microanalysis, 3rd edn. Springer, New York
15. Invitation to the SEM World JEOL Ltd. Publication, Tokyo, Japan. https://wiki.nbi.ku.dk/w/cleanroom/images/b/b5/Invitation_to_the_SEM_World.pdf. Date accessed 19 Sept 2018
16. Joy DC (1998) Scanning electron microscopy. In: Amelinckx S, van Dyck D, van Landuyt J, van Tendeloo G (eds) Handbook of microscopy-applications. VCH, Weinheim
17. Ball MD, Wilson M, Whitmarsh S (1987) In: Brown LM (ed) Electron microscopy and microanalysis 1987. Institute of Physics, London, p 185
18. Tixier J, Philibert R (1969) Effets de contraste cristallin en microscopie électronique à balayage. Micron (1):174
19. Seiler H (1967) Einige aktuelle Probleme der Sekundarelektron-emission. Z Phys 22:249–263
20. Koshikawa T, Shimizu R (1974) A Monte Carlo calculation of low-energy secondary electron emission from metal. J Phys D Appl Phys 7:1303
21. Drescher H, Reimer L, Seidel H (1970) Rückstreukoeffizient und Sekundärelektronen-Ausbeute von 10–100 keV-Elektronen und Beziehungen zur Raster-Elektronenmikroskopie. Z Agnew, Phys 29:331–336
22. Loretto MH (1984) Electron beam analysis of materials. Chapman and Hall, London
23. Reimer L, Tollkamp C (1980) Measuring the backscattering coefficient and secondary electron yield inside a scanning electron microscope. Scanning 3(1):35–39
24. Joy DC (1987) A model for calculating secondary and backscattered electron yields. J Microsc 147(1):51–64
25. Vaz OW, Krause SJ (1986) In Proc. EMSA Conference Bailey GW (ed), San Francisco Press, San Francisco, p. 676
26. Wittry DB (1966) Proc: 4th international conference on X-ray optics and microanalysis, Castaing R, Deschamps P, Philibert J (eds) Hermann, Paris, p. 168
27. Kanter H (1961) Energy dissipation and secondary electron emission in solids. Phys Rev 121 (3):677–681
28. Bozolla JJ (1999) Electron microscopy, principles and techniques for biologists, 2nd edn. Jones and Bartlett Publishers, Burlington